Graz University of Technology

Master Thesis

Multi-target Tracking for UWB Channels Using PHD Filters

conducted at the
Signal Processing and Speech Communication Laboratory
Graz University of Technology, Austria

by
Markus Fröhle

Supervisors:
Assoc.Prof. Dipl.-Ing. Dr. Klaus Witrisal
Dipl.-Ing. Paul Meissner

Graz, December 2011

Statutory Declaration

I declare that I have authored this thesis independently, that I have not used other than the declared sources/resources, and that I have explicitly marked all material which has been quoted either literally or by content from the used sources.

date	(signature)

Abstract

In this thesis, the applicability of a multi-source multi-target Bayes filter is evaluated with respect to its ability to extract and track multipath components (MPCs) in measured indoor ultra-wideband (UWB) channels. The measurements of the channel impulse responses (CIRs) were obtained along a reference trajectory of a mobile transmitter station in a realistic indoor environment. The probability hypothesis density (PHD) filter is used, which approximates the multi-target posterior probability density function by its multi-target first order statistical moment and propagates it in time. Two implementations of this filter are considered, a sequential Monte-Carlo (SMC) and a Gaussian mixture (GM) approach.

The characteristics of the implementations are discussed and performance evaluations are done both using simulated data and the measured CIRs. The first case allows for a detailed evaluation of model mismatches, such as target motion which is not following the linear constant-velocity model that is used for target dynamics. In the second case, it is shown that the multipath extraction problem is especially challenging due to diffuse scattered components in the measurements and their distribution in the state space.

Performance results show the applicability of the filter if the assumptions made on target dynamics and clutter distributions fit well with the measurement set. Important performance parameters are identified using real measurement data and important directions for future work are given.

Keywords

UWB, multi-target filtering, PHD-Filter, FISST, RFS, Sequential Monte-Carlo, Gaussian mixture, statistical information fusion

Kurzfassung

Die vorliegende Arbeit beschäftigt sich mit der Evaluierung eines Multihypothesenfilters, dem probability hypothesis density (PHD) Filter, zur Erfassung und Verfolgung der Komponenten der Mehrwegausbreitung (MPCs) basierend auf Ultrabreitbandkanalimpulsantworten eines Innenraumes, welche entlang einer Trajektorie aufgenommen wurden. Die Messungen sind dabei überlagert von diffusen Störkomponenten und vorherrschendem Messrauschen.

Der verwendete Filter approximiert die a-posteriori Wahrscheinlichkeitsdichtefunktion des Hypothesenraumes anhand des statistischen Momentes erster Ordnung und propagiert diese zeitlich weiter. Die Zustandsänderung soll einem konstantem Beschleunigungsmodell folgen. Diese Vereinfachungen reduzieren das Anwendungsbebiet des Filters. Der Filter selbst schätzt zwar die Anzahl der vorhandenen Zustände, gibt sie jedoch nicht direkt aus. Daher müssen diese noch extrahiert und einem Pfad zugeordnet werden.

Zwei Implementierungen des PHD-Filters, eine sequentielle Monte-Carlo Variante sowie eine Implementierung, welche Gauß'sche Mischverteilungen verwendet, werden untersucht. Zunächst auf simulierten Messwerten um deren Eigenschaften zu bestimmen, dann mit den Ultrabreitbandmessungen. Es zeigt sich, dass das verwendete Multihypothesenfilter sowohl die Anzahl als auch die vorhandenen Zustände hinreichend genau schätzen kann. Jedoch unter der Bedingung, dass die Annahmen der Zustandsverteilung und deren Änderung auch dem verwendeten Modell entsprechen. Andernfalls ist die Filterleistung nicht zufriedenstellend.

Stichwörter

Ultrabreitband, Multihypothesenfilter, PHD-Filter, FISST, RFS, Monte-Carlo, Gauß'sche Mischverteilung

Acknowledgement

I would like to show my gratitude to my supervisors, Paul Meissner and Klaus Witrisal, whose encouragement, guidance and support made this thesis possible.

Markus Fröhle

Contents

List of Figures

List of Tables

List of Abbreviations & Symbols

Abbreviations

BS base station

cdf cumulative distribution function

CIR channel impulse response

CPHD cardinalized PHD

FCC Federal Communications Commission

FISST finite-set statistics

GM Gaussian mixture

GMM Gaussian mixture modelling

GPS global positioning system

i.i.d. independent and identically distributed

IDFT inverse Fourier transform

JPDA joint probabilistic data association

LASER light amplification by stimulated emission of radiation

LOS line-of-sight

MHT multi hypothesis tracking

MPC multi-path component

MS mobile station

NLOS non line-of-sight

OSPA optimal sub-pattern assignment

pdf probability density function

PF particle filter

PHD	probability hypothesis density
RFS	random finite set
SLAM	simultaneous localization and mapping
SMC	sequential Monte Carlo
SNR	signal-to-noise ratio
UWB	ultra wideband

Symbols

$[\alpha]_{\max}$	maximum value in the corresponding domain, e.g. α
$[\alpha]_{\min}$	minimum value in the corresponding domain, e.g. α
α	amplitude
$\Delta\alpha$	amplitude difference
$\Delta\tau$	delay difference
Γ_k	system state RFS
κ_k	intensity of clutter RFS K_t
λ	parameter of Poisson distribution
$\mathbf{x}_k$	(multi-dimensional) target state
$\mathbf{z}_k$	(multi-dimensional) measurement
Σ_k	measurement RFS
$\sigma^2_{[\alpha],\mathbf{n}}$	SMC PHD-Filter process noise variance in the corresponding domain, e.g. α
$\sigma^2_{[\alpha],\mathrm{B}}$	GM PHD-Filter birth RFS variance in the corresponding domain, e.g. α
$\sigma^2_{[\alpha],\mathrm{b}}$	SMC PHD-Filter particle birth variance in the corresponding domain, e.g. α
$\sigma^2_{[\alpha],\mathrm{L}}$	SMC PHD-Filter measurement-state likelihood variance in the corresponding domain, e.g. α
$\sigma^2_{[\alpha],\mathrm{Q}}$	GM PHD-Filter process noise variance in the corresponding domain, e.g. α
$\sigma^2_{[\alpha],\mathrm{R}}$	GM PHD-Filter measurement noise variance in the corresponding domain, e.g. α
$\sigma^2_{[\alpha]}$	variance in the corresponding domain, e.g. α
τ	delay

B_{thresh} target labelling likelihood

c cut-off parameter of OSPA multi-target miss distance

$D_{k+1|k+1}$ prior PHD of some RFS with the probability distribution of $p_{\Gamma_{k+1}|\Sigma_{1:k+1}}(X_{k+1}|Z_{1:k+1})$, the posterior multi-target pdf in time step $k+1$

$D_{k+1|k}$ PHD of some RFS with the probability distribution of $p_{\Gamma_{k+1}|\Sigma_{1:k}}(X_{k+1}|Z_{1:k})$, the prior multi-target pdf

E_O observation space

E_S system-state space

K_k clutter RFS in time-step k

M number of newborn particles per time-step

N_0 number of particles per object

N_{R} total number of time-steps

p order parameter of OSPA multi-target miss distance

P_{D} probability of detection

P_{S} probability of survival

$p_{\Gamma_{k+1}|\Sigma_{1:k}}(X_{k+1}|Z_{1:k})$ the prior multi-target pdf

$p_{\Gamma_{k+1}|\Sigma_{1:k+1}}(X_{k+1}|Z_{1:k+1})$ the posterior multi-target pdf in time step k

$p_{\Gamma_k|\Sigma_{1:k}}(Z_k|X_k)$ the multi-target likelihood

X_k target state set

Z_k measurement set

1 Introduction

Robust and reliable systems for localization are of special interest in various areas. In outdoor scenarios, this problem has been solved by satellite based systems like the global positioning system (GPS). In indoor scenarios, GPS can not be used due to the lack of a line-of-sight (LOS) path which is required for it. Also many indoor localization approaches utilize sensing techniques based on the LOS path, i.e. light amplification by stimulated emission of radiation (LASER) or ultra-sound. Based on this, sophisticated localization methods have been developed, e.g. simultaneous localization and mapping (SLAM) [DWB06, BDW06]. A quite promising sensing technology for indoor localization is to make use of ultra wideband (UWB) signals. Such signals benefit of having a large freely available bandwidth of $3.1 - 10.6$ GHz according to Federal Communications Commission (FCC) regulations. This large bandwidth manifests itself in a fine spatial resolution of only 4cm [Mol09] in all propagation paths. In contrast to this, the spatial resolution of LASER is superior but only for one observation point. Multiple measurements are needed to sense the whole observation space. In the case of UWB, multipath propagation can be resolved. Multipath propagation is a phenomenon where the transmitted signal reaches the receiver not only on the direct path, but also on multiple paths which are caused by the wave being reflected or scattered at, e.g. room walls, before arriving at the receiver [SW09]. The different path lengths of the multi-path components (MPCs) lead to different arrival times at the receiver side. A distinguishing feature of UWB is that many of these individual paths are recognizable and resolvable in the measurements [KP03],[HRV11].

Many localization schemes utilize multilateratation of three or more reference nodes to estimate the position. In situations where the LOS path is blocked, schemes based on this tend to be error prone. Methods which overcome this can e.g. incorporate MPCs for localization [MSW10]. Here, MPCs are assigned to virtual sources placed at the distance and direction of the impinging MPC at the receiver side. In fact, if floor plan information is available, robust

and accurate indoor localization is possible with only one reference node [MAGW11]. However, these methods still lack an efficient and accurate method for extracting MPCs from the measurements. [SKA+08] and [SKA+10] presented a method for extracting MPCs from UWB channel impulse responses (CIRs) in an outdoor scenario. They are then assigned to scatterer locations in the spatial domain. This has been adapted to estimate virtual sources in an indoor scenario [FMGW11]. However, to perform online localization, these MPC extraction methods are not applicable. For this purpose, an online method for extraction and tracking of MPCs needs to be developed.

1.1 Outline

The remainder of this section describes the UWB channel model used, the motivation of this work and the indoor measurement campaign. In Section 2, optimal single- and multi-target Bayes filtering is discussed. Section 3 deals with the approximations of the optimal multi-target filtering and introduces the PHD-Filter together with its two implementations. Section 4 describes multi-target miss-distances. The evaluation of the filter implementations on simulated and real measurement data is discussed in Section 5. Finally, in Section 6 a conclusion of the results obtained is given.

1.2 Channel Model

A model for the UWB-CIR is given as [Mol05]

$$h(\tau) = \sum_{i=1}^{N} \alpha_i \chi_i(\tau) \otimes \delta(\tau - \tau_i). \tag{1.1}$$

Here, α_i denotes a scalar weighting factor, $\chi_i(\tau)$ denotes the distortion of the i-th MPC by the frequency selectivity of interaction objects, $\delta(\tau - \tau_i)$ is the time delay of the i-th MPC and $\otimes$ is the convolution operator. The distortion factor $\chi_i(\tau)$ is often unknown.

A simplification of this model leads to a tapped delay line model. Such a simplified model for the CIR assuming a mobile agent at position $\mathbf{p}_k$ is given by [MAGW11]

$$h_k(\tau) = \sum_{l=1}^{L_k} a_{k,l} \delta(\tau - \tau_l) + v_k(\tau) + n_k(\tau). \tag{1.2}$$

The CIR $h_k(\tau)$ is a summation of L_k deterministic, specular reflections; diffuse scattering components $v_k(\tau)$ and the measurement noise $n_k(\tau)$. $a_{k,l}$ is the complex-valued amplitude of the l-th deterministic, specular reflection. We are interested in estimating and tracking of these deterministic, specular reflections (the MPCs) from the UWB-CIR measurements.

1.3 Motivation

Within this work, a suitable method for tracking MPCs in indoor UWB-CIR measurements shall be evaluated.

The method used has to cope with:

- the number of MPCs present in the measurements L_k is unknown and has to be estimated
- L_k varies for different positions $\mathbf{p}_k$ of the MS
- the measurements are superimposed by $v_k(\tau)$ and $n_k(\tau)$

Within this work, the applicability of a multi-source multi-target filter, the probability hypothesis density (PHD) Filter, is evaluated with respect to its ability to extract and track MPCs in indoor UWB CIR measurements gathered along a MS trajectory. As the PHD-Filter does not produce target tracks, a sophisticated method of target track estimation has to be used. Furthermore, the indoor UWB measurements have to be preprocessed in an adequate manner, before they can be utilized as inputs for the multi-target PHD-Filter.

1.4 Indoor Measurement Campaign

The indoor UWB measurement campaign took place at a hallway located at the department of the Signal Processing and Speech Communication Laboratory at Graz, University of Technology. The measurement setup is given in Tab. 1.1 and the floor plan is plotted in Fig. 1.2. The walls of the hallway are made of concrete. The hallway has large glass fronts with small metal pillars located in front of them. Another pillar made of concrete is located close to the position of the receiver base station. In the floor plan the receiver base station (BS) is marked with BS 3. The transmitter mobile station (MS) is moving along the illustrated trajectory. The trajectory of the MS is composed of 381 positions spaced by 10cm. For every MS position, the complex channel transfer function in the frequency range of $6 - 8$GHz was measured with a vector network analyser with 1MHz spacing. The CIRs are computed using the inverse discrete Fourier transform (IDFT) of the complex channel transfer function with a certain amount of oversampling and are plotted along the MS trajectory in Fig. 1.1. In the figure the amplitude of the single CIRs is encoded in colour. The LOS component is clearly visible having the lowest delay and the highest amplitude along the MS trajectory. Also some MPCs with a higher delay than the LOS component caused by single and double reflections are visible. In the non line-of-sight (NLOS) situation (MS position 280 to 320) no LOS component and also almost zero specular MPCs are present. Additional details can be found in [FMGW11, MAGW11]. The measurements are preprocessed beforehand following the method explained in [MAGW11]. The preprocessing step is explained in Section 5.3.1.

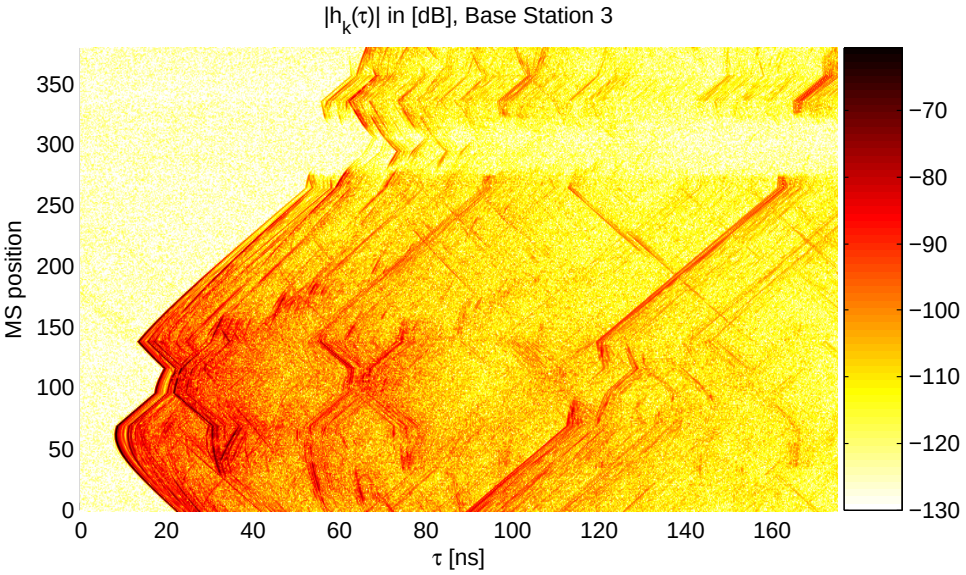

Figure 1.1: Measured CIRs along the MS position trajectory

Parameter	**Value**
Scenario	Indoor hallway with concrete walls, large glass fronts and metal pillars
No. of MS positions	381, spacing 10 cm
Frequency range	6 − 8 GHz
Frequency spacing	1 MHz
Network Analyzer	Rhode & Schwarz ZVA-24
Antennas	Skycross SMT-3TO10M plus custom made 5-cent coin antenna
Antenna height	1.5 m

Table 1.1: Measurement Setup of indoor measurement campaign

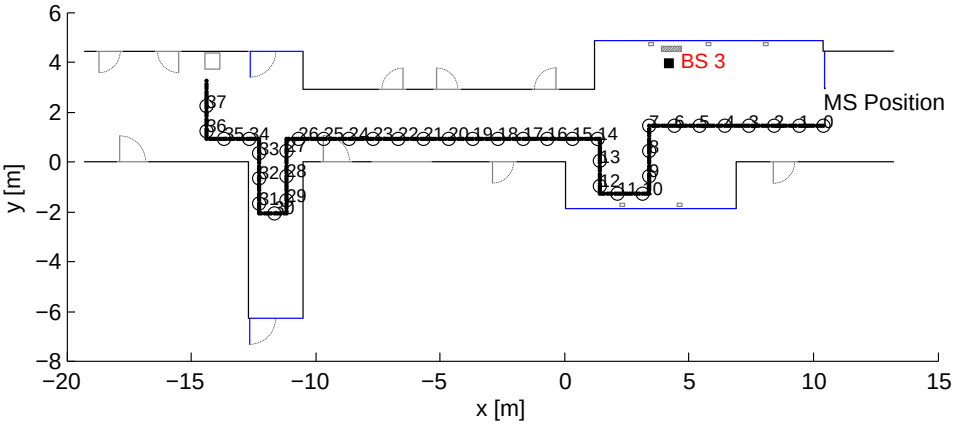

Figure 1.2: Floor plan and measurement trajectory of the MS

1.5 Related Work

In [YSK+08], a method for tracking MPCs utilizing particle filters (PFs) was established. This method is restricted to the case where no path overlap occurs. Then, tracking of multiple MPCs can be performed simultaneously with multiple parallel PFs, one for each MPC. In a real world scenario the assumption of no path overlap is likely to be violated. Furthermore, the number of MPCs present in the measurements varies, which has to be handled separately.

Another possibility is to use an multi-source multi-target filtering approach for tracking MPCs in succeeding time-steps [BSL95]. One filtering technique capable of maintaining multiple target tracks is the multi hypothesis tracking (MHT) filter [Rei79]. It maintains multiple hypotheses of the association between a target state and the measurement in the measurement set [PVSD04]. The drawback of MHT is the exponentially growing number of hypotheses over time [PVSD04]. Another method is the joint probabilistic data association (JPDA) filter. It approximates the posterior target distribution as separate Gaussian distributions for each target [SVL04, BSL95]. The Rao-Blackwellized Monte Carlo data association algorithm for multi-target tracking partitions the multi-target tracking problem into the estimation of the posterior distribution of the data associations and the estimation of the single target tracking sub-problems solved by a Kalman filter [SVL04, SVL07]. Special assumptions on clutter appearance, target dynamics and prior distributions of target states are needed.

Another proposed approach called the PHD-Filter is based on finite-set statistics (FISST) theory [Mah04, Mah01, Mah03, Mah07b]. This multi-source multi-target filter does not produce direct target tracks and therefore avoids the target-measurement association problem. The PHD-Filter propagates the PHD, a first order moment of the multi-target posterior, in time. The single-target counterpart to the PHD is the mean value. The PHD-Filter is the multi-target counterpart to the constant-gain Kalman filter [Mah03]. Several implementations of the PHD-Filter based on a sequential Monte Carlo implementation exist [Sid03, VS03, CB07, RCV10]. If target movement is restricted to Gaussian dynamics, a closed-form solution of the PHD recursion exist [VM06] and several Gaussian mixture implementations have been established [VM05, VM06, CPV06, PCV09].

The PHD-Filter confines the propagation of the full multi-target posterior to the first order multi-target moment which corresponds to a loss of information [Mah07b]. Propagating the whole multi-target posterior is up to now computationally intractable. The CPHD-Filter (cardinalized PHD) additionally propagates the cardinality distribution to the PHD and leads to better performance [Mah07b, Mah07a, VVC06]. This is still a simplification to the propagation of the first and second order multi-target moment of the multi-target posterior.

2 Bayes Filtering

2.1 Tracking of a Single Target

2.1.1 Problem Definition

A physical process that changes over time is mathematically referred as a dynamical system. Observing the system's state at discrete time steps allows the description of the dynamical system by difference equations. A system model is needed to describe the behaviour of the physical process mathematically. Let $\mathbf{x_k} = [x_{k,1}, \ldots, x_{k,\mathrm{N}}]^{\mathrm{T}}$ be the N-dimensional system state at discrete time step k . Then the system can be described by the difference equation [AMGC02]

$$\mathbf{x}_k = f_k(\mathbf{x}_{k-1}, \mathbf{v}_{k-1}). \tag{2.1}$$

The system state $\mathbf{x}_k$ is determined by a possibly non-linear function $f_k(\cdot)$, the independent and identically distributed (i.i.d.) noise sequence $\mathbf{v}_{k-1}$ and the system state $\mathbf{x}_{k-1}$ of the previous time-step $k-1$. Note, for this equation to hold the first order Markov assumption has to be considered [BN07], i.e.

$$p(\mathbf{x_k}|\mathbf{x_{k-1:1}}) = p(\mathbf{x_k}|\mathbf{x_{k-1}}). \tag{2.2}$$

That means the probability of the system state $\mathbf{x}_k$ in time step k only depends on the state $\mathbf{x}_{k-1}$ in the previous time step $k-1$ and not on the whole history of past states $\mathbf{x}_{1:k-2}$. In a physical system the state vector $\mathbf{x}_k$ often cannot be directly measured. Furthermore, the measurement may be affected by noise or other distorting effects causing the measurement being only a noisy observation of the system state $\mathbf{x}_k$ at time step k. Putting the measurement into relation with

the system state yields

$$\mathbf{z}_k = h_k(\mathbf{x}_k, \mathbf{n}_k). \tag{2.3}$$

Here, $h_k(\cdot)$ is a possibly non-linear function of the state $\mathbf{x}_k$ and $\mathbf{n}_k$ is an i.i.d. noise sequence; e.g. the system state vector could be $\mathbf{x}_k = [\alpha, \tau, \Delta\alpha, \Delta\tau]^{\mathrm{T}}$ and the measurement vector could be $\mathbf{z}_k = [\alpha, \tau]^{\mathrm{T}}$, where α denotes the amplitude, τ the delay and $\Delta\alpha, \Delta\tau$ their changes from the previous to the current time step.

2.1.2 Optimal State-space Filter

We are interested in estimating the system state $\mathbf{x_k}$, given all the measurements $\mathbf{z_{1:k}} = \{z_i | i = 1, \ldots, k\}$ up to time k. From a probabilistic point of view, this corresponds to estimating the posterior probability density function (pdf) $p(\mathbf{x}_k|\mathbf{z}_{1:k})$. The computation of the posterior pdf can be split up into a prediction and an update step. The Chapman-Kolgomorov equation [AMGC02] describes the prediction step and is given by

$$p(\mathbf{x}_k|\mathbf{z}_{1:k-1}) = \int p(\mathbf{x}_k|\mathbf{x}_{k-1}) p(\mathbf{x}_{k-1}|\mathbf{z}_{1:k-1}) d\mathbf{x}_{k-1}. \tag{2.4}$$

Here, $p(\mathbf{x}_k|\mathbf{z}_{1:k-1})$ is called the prior pdf, $p(\mathbf{x}_k|\mathbf{x}_{k-1})$ describes the state propagation from the previous time step $k-1$ to the current time step k and $p(\mathbf{x}_{k-1}|\mathbf{z}_{1:k-1})$ is the posterior pdf in time step $k-1$. The update equation computes the posterior pdf and can be inferred using Bayes' law [BN07], namely [Sim06]

$$p(\mathbf{x}_k|\mathbf{z}_{1:k}) = \frac{p(\mathbf{z}_k|\mathbf{x}_k) p(\mathbf{x}_k|\mathbf{z}_{1:k-1})}{p(\mathbf{z}_k|\mathbf{z}_{1:k-1})}. \tag{2.5}$$

Here, $p(\mathbf{z}_k|\mathbf{x}_k)$ is the likelihood of the measurement $\mathbf{z}_k$ conditioned on the system state $\mathbf{x}_k$ and the prior pdf $p(\mathbf{x}_k|\mathbf{z}_{1:k-1})$ was obtained in the prediction step. It is divided by the marginal distribution $p(\mathbf{z}_k|\mathbf{z}_{1:k-1})$ of receiving measurement $\mathbf{z}_k$ knowing all the previous measurements $\mathbf{z}_{1:k-1}$. This constant is obtained by

$$p(\mathbf{z}_k|\mathbf{z}_{1:k-1}) = \int p(\mathbf{z}_k|\mathbf{x}_k) p(\mathbf{x}_k|\mathbf{z}_{1:k-1}) d\mathbf{x}_k \tag{2.6}$$

and depends on the likelihood $p(\mathbf{z}_k|\mathbf{x}_k)$ and the process noise, both defined by the system model (2.3).

2.1.3 Optimal Implementation

The computation of the whole posterior pdf in (2.5) cannot be determined analytically [AMGC02], unless special assumptions are made. In the case of the Kalman filter the posterior pdf in any time-step is a Gaussian distribution, which is fully described by its mean and variance [AMGC02]. This implies certain restrictions on the system: The function $f_k(\cdot)$ given in (2.1) and $h_k(\cdot)$ in (2.3) are linear functions; the initial state $\mathbf{x}_0$, the process noise $\mathbf{v}_{k-1}$ and measurement noise $\mathbf{n}_k$ follow a zero mean multivariate Gaussian distribution [Kal60, WB01].Then a

closed form solution for the posterior pdf exists.

2.1.4 Approximate Implementation

If the assumptions made in the case of the Kalman filter are not satisfied, the computation of the posterior pdf has to be approximated numerically. One such approximate method is the particle filter [Sim06, AMGC02]. It samples the posterior pdf and propagates the samples instead of the whole pdf. These samples are distributed according to the posterior pdf $p(\mathbf{x}_k|\mathbf{z}_{1:k})$. For linear Gaussian dynamics the ideal solution of the particle filter reduces to the Kalman filter [Sim06].

2.2 Tracking of Multiple Targets

In the multi-target case, zero or more targets are present. The targets appear and disappear randomly in the state-space. If a target is present, its state-space model equals the single target case (2.1). Also the generated observation by the i-th target with state $\mathbf{x}_{k,i}$ equals (2.3).

The set X_k holds all the targets which are present in time step k and is, according to [PVSD04], defined as

$$X_k = \{\mathbf{x}_{k,1}, \mathbf{x}_{k,2}, \ldots, \mathbf{x}_{k,M(k)}\} \subset E_S. \tag{2.7}$$

Here, $M(k)$ is the number of present targets at time-step k. E_S is the state-space. The received measurements in time-step k are also put into a set

$$Z_k = \{\mathbf{z}_{k,1}, \mathbf{z}_{k,2}, \ldots, \mathbf{z}_{k,N(k)}\} \subset E_O. \tag{2.8}$$

Here, $N(k)$ is the number of received measurements in time-step k. The received measurement set Z_k is a subset of the observation space E_O. It is assumed that not every measurement has its origin in a state $\mathbf{x}_{k,i}$. Due to clutter, some measurements $\mathbf{z}_{k,j} \in Z_k$ might be present although they do not origin from an underlying state $\mathbf{x}_{k,i} \in X_k$. This spurious measurements are modelled by a specific clutter model [PVSD04].

Random Finite Set Formulation

To represent uncertainty about the number of elements in the multi-target state X_k and measurement Z_k, both are modelled by random finite sets (RFSs) [Sid03]. A RFS X is a finite-set valued random variable, which can be described by a discrete probability distribution and a family of joint probability densities [VM06]. The discrete distribution describes the cardinality of X and an appropriate density characterizes the joint distribution of the elements in X [VM06].

For the further discussion, let $\Gamma_k = \{\mathbf{X}_{k,1}, \mathbf{X}_{k,2}, \ldots, \mathbf{X}_{k,M(k)}\}$ be a RFS. A certain outcome is then denoted by X_k given in (2.7). Similarly for the measurements, let $\Sigma_k = \{\mathbf{Z}_{k,1}, \mathbf{Z}_{k,2}, \ldots, \mathbf{Z}_{k,N(k)}\}$ be a RFS. A certain outcome is then denoted by Z_k given in (2.8).

Definition of the Filtering Problem

The objective of a multi-target state-space estimator is to estimate the unobserved system state sets $X_{1:k} = \{X_i | i = 1, \ldots, k\}$ up to time k, given the sets of observations $Z_{1:k} = \{Z_i | i = 1, \ldots, k\}$, i.e., obtain $\hat{X}_k = \{\hat{\mathbf{x}}_{k,1}, \hat{\mathbf{x}}_{k,2}, \ldots, \hat{\mathbf{x}}_{k,\hat{T}_k}\}$, where $\hat{\mathbf{x}}_{k,i}$ are the individual target estimates and $\hat{T}_k$ is the estimate of the number of targets in $\hat{X}_k$ at time k [CB07].

Optimal State-space Filter

With the random finite set formulation given in Section 2.2, it is possible to formulate the multi-target tracking problem within the Bayesian framework [PVSD04]. Assume that $Z_{1:k} = \{Z_i | i = 1, \ldots, k\}$ is the set of all measurements received up to time k, then the multi-target posterior, as a counterpart of the single target posterior in (2.5) is defined by [Sid03]

$$p_{\Gamma_k|\Sigma_{1:k}}(X_k|Z_{1:k}) \propto p_{\Sigma_k|\Gamma_k}(Z_k|X_k) p_{\Gamma_k|\Sigma_{1:k-1}}(X_k|Z_{1:k-1}). \tag{2.9}$$

Here, $p_{\Gamma_k|\Sigma_{1:k}}(X_k|Z_{1:k})$ is the multi-target posterior density, $p_{\Sigma_k|\Gamma_k}(Z_k|X_k)$ the multi-target likelihood and $p_{\Gamma_k|\Sigma_{1:k-1}}(X_k|Z_{1:k-1})$ the multi-target prior density. To describe these densities a mathematical framework called finite-set statistics is needed [Sid03].

Finite-set statistics

For an introduction on FISST see [Mah04, Mah01, Mah07b]. The aim of FISST is to transform multisensor-multitarget problems into single-sensor single-target problems mathematically by bundling all sensors into a single "meta-sensor", all targets into a single "meta-target" and all observations into a single "meta-observation" [Mah04]. This transformation is illustrated in Fig. 2.1. The solution of the multisensor-multitarget problem within the FISST framework is then mathematically equivalent to the single-sensor single-target problem.

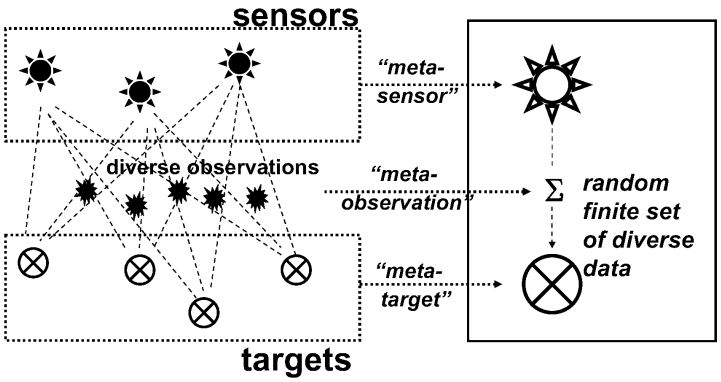

Figure 2.1: Illustrates the basic concept of FISST theory. Source: [Mah04]

The connection between the single target case and the multi-target case are collected in table 2.1.

Single Target	**Multiple Target**
sensor	meta-sensor
target	meta-target
vector observation $\mathbf{z}$	finite-set observation Z
vector state $\mathbf{x}$	finite-set state X
derivative	set-derivative
integral	set-integral

Table 2.1: Connection between single-target problems and multi-target exploiting FISST theory. Source: [Mah04]

3
Approximate Multi-target Filtering

In single-target filtering, propagating the full posterior pdf $p(\mathbf{x}_k|\mathbf{z}_{1:k})$ is only possible if certain assumptions on target dynamics are made (see Section 2.1.3). In cases where these assumptions are not fulfilled, suitable approximations have been developed (see Section 2.1.4). Optimal Bayes multi-target filtering propagating the full multi-target posterior density in time is computationally intractable. The multi-target posterior needs to be approximated by its statistical moments and then they are propagated in time instead [PVSD04]. Let us redefine the approximations of the posterior pdf made in the single-target case in order define the approximations necessary in the multi-target posterior pdf.

The first order moment vector and the second order moment matrix are given by

$$\mathrm{E}\{\mathbf{x}_k\} = \int \mathbf{x}_k \; p(\mathbf{x}_k|\mathbf{z}_{1:k}) d\mathbf{x}_k \tag{3.1}$$

and

$$C_k = \int \mathbf{x}_k \mathbf{x}_k^{\mathrm{T}} \; p(\mathbf{x}_k|\mathbf{z}_{1:k}) d\mathbf{x}_k, \tag{3.2}$$

respectively [Mah03]. Here, $p(\mathbf{x}_k|\mathbf{z}_{1:k})$ is the single-target posterior density, $\mathbf{z}_{1:k}$ is the set of all measurements up to time k. The operator $[\cdot]^{\mathrm{T}}$ denotes a matrix transpose. $\mathrm{E}\{\cdot\}$ is the expectation operator. If the posterior pdf is assumed to follow a multi variate Gaussian distribution, higher order moments can be neglected. The posterior pdf is then fully described by the first and second order moments. The Kalman filter, which propagates these two moments in time, is then the optimal solution to this single target filtering problem (see Section 2.1.3).

If the likelihood of the measurement-state, $p(\mathbf{z}_k|\mathbf{x}_k)$, is unimodal, and has a small covariance, it usually can be reasonably approximated with a Gaussian pdf. If furthermore the variance is low, even an approximation with only the first order moment might be enough. Then the second

order moment can be neglected as well and it suffices to only propagate the first order moment, because $p(\mathbf{x}_k|\mathbf{z}_{1:k}) \cong p(\mathbf{x}_k|\mathrm{E}\{\mathbf{x}_k\})$ [Mah03]. An example for such a filter is the constant gain Kalman filter.

In the following the idea of only propagating the first order statistical moment is expanded to the multi-target filtering problem. Then the multi-target first order statistical moment $D_{k|k}$ gives a sufficient statistic to approximate the multi-target posterior pdf

$$p_{\Gamma_k|\Sigma_{1:k}}(X_k|Z_{1:k}) \cong p_{\Gamma_k|\Sigma_{1:k}}(X_k|D_{k|k}). \tag{3.3}$$

The definition of a multi-target first order statistical moment will be given in Section 3.1. The full posterior can only be approximately recovered from the first order moment if the signal-to-noise ratio (SNR) is high and the targets move independently from each other [Sid03]. Then the multi-target filtering problem simplifies from multi-target pdf propagation to first order moment propagation like it is illustrated in Tab. 3.1 [Mah03]. The first row indicates the prediction and update of the multi-target pdf and the second row indicates the prediction and update of the first order multi-target moment.

$p_{\Gamma_k\|\Sigma_{1:k}}(X_k\|Z_{1:k})$	$\rightarrow$	$p_{\Gamma_{k+1}\|\Sigma_{1:k}}(X_{k+1}\|Z_{1:k})$	$\rightarrow$	$p_{\Gamma_{k+1}\|\Sigma_{1:k+1}}(X_{k+1}\|Z_{1:k+1})$
$\downarrow$	predict	$\downarrow$	update	$\downarrow$
$D_{k\|k}$	$\rightarrow$	$D_{k+1\|k}$	$\rightarrow$	$D_{k+1\|k+1}$

Table 3.1: Simplification of multi-target filtering problem from posterior pdf propagation to first order moment propagation. Source: [Mah03]

3.1 The Probability Hypothesis Density

3.1.1 Definition

The first order moment of a random finite set Ξ is called the probability hypothesis density D_Ξ and is given by [PVSD04]

$$D_\Xi(\mathbf{x}) = \mathrm{E}\{\delta_\Xi(\mathbf{x})\}. \tag{3.4}$$

Here, $\mathrm{E}\{\cdot\}$ denotes the expectation operator and

$$\delta_\Xi(\mathbf{x}) = \sum_{\mathbf{x}\in\Xi} \delta_{\mathbf{x}} \tag{3.5}$$

is the random density representation of the random finite set Ξ for each $\mathbf{x} \in \Xi$. The random density representation equals the summation of Dirac delta functions $\delta_{\mathbf{x}}$, which are centred at the values of $\mathbf{x}$.

The PHD D_Ξ has the following properties [PVSD04]:

- the peaks of the PHD $D_\Xi(\mathbf{x})$ give the estimates of the elements of Ξ,

- the PHD $D_{\Xi}(\mathbf{x})$ is a unique function on the space E where the individual targets exist. Its integral $\int_S D_{\Xi}(\mathbf{x})d\mathbf{x}$ over a measurable subset $S \subseteq E$ yields the expected number of elements of Ξ in S.

3.1.2 Poisson Approximation

In order to hold that the PHD $D_{k|k}$ and $D_{k+1|k}$ of $p_{k|k}(X|Z^k)$ and $p_{k+1|k}(X|Z^k)$ are "best-fit" approximations, which means the Kullback-Leibler information functionals are minimized, the multi-target posterior $p_{k+1|k}(X|Z^k)$ has to be approximately Poisson distributed. This also means that the predictor $D_{k|k} \rightarrow D_{k+1|k}$ is lossless, whereas the corrector $D_{k+1|k} \rightarrow D_{k+1|k+1}$ is not lossless [Mah03]. A proof is given in [Mah03].

3.2 PHD-Filter

The PHD-Filter propagates the multi-target first order moment, the PHD, forward in time. The number of targets and their positions can be estimated in each time step from the PHD. It does not make any data association and therefore lacks of tracking the targets identity [CB07]. If the target identities are also of interest a data association algorithm as to be put on top of it. A data association algorithm is discussed in Section 3.3.

3.2.1 Definition

First, an RFS model for the system state set X_k and the measurement set Z_k is defined. This model incorporates target motion, birth and death. Then, the PHD-Filter, consisting of the prediction and the update step, operating on this model is defined. The definition of the PHD-Filter is given in [CB07] and restated here.

System State Set

The system state set X_k is a RFS whose elements within the set have three different origins. It is composed of [VM06]

$$X_k = \left(\bigcup_{\mathbf{x} \in X_{k-1}} S_{k|k-1}(\mathbf{x}) \right) \cup \left(\bigcup_{\mathbf{x} \in X_{k-1}} B_{k|k-1}(\mathbf{x}) \right) \cup \Gamma_k. \tag{3.6}$$

Here, $S_{k|k-1}(\mathbf{x})$ is a RFS containing the surviving targets from the previous system state set X_{k-1}. $B_{k|k-1}(\mathbf{x})$ is a RFS of spawned targets. Spawned targets occur if one target state $\mathbf{x}$ forks into two new target states in the next time-step. For simplicity, spawned targets will be omitted in this work. Γ_k is a RFS of new targets occurring in this time-step. The system state RFS X_k is then a union of target states having these three different origins.

Measurement Set

The measurement set Z_k is a RFS and is a union of measurements, which origin from system states and false-alarms measurements caused by clutter. It is described by [VM06]

$$Z_k = K_k \cup \left(\bigcup_{\mathbf{x} \in X_k} \Theta_k(\mathbf{x}) \right). \tag{3.7}$$

Here, K_k is a RFS containing false-alarms measurements originated from clutter and $\Theta_k(\mathbf{x})$ is a RFS of measurements originated from system states in the system state set X_k. The actual model for the clutter RFS is problem-dependent. The intensity of the clutter measurement RFS is given by

$$\kappa_k(\mathbf{z}) = \lambda_k u_k(\mathbf{z}). \tag{3.8}$$

For the PHD-Filter, the number of false alarms within the measurement set Z_k are assumed to be Poisson distributed with the Poisson parameter λ_k [Mah03]. Also the number of false-alarms does not change over time, i.e. $\lambda_k = \lambda$. $u_k(\mathbf{z})$ is the probability density of false-alarms within the measurement set. Also this density does not change over time, i.e. $u_k(z) = u(z)$. For simplicity, the probability density of false-alarms is chosen as a uniform distribution over the whole state-space $u_k(\mathbf{z}) \sim \mathrm{U}$.

Prediction Step

The predicted prior PHD $D_{k|k-1}(\mathbf{x}_k|Z_{1:k-1})$ for a target state $\mathbf{x}_k \in X_k$, given all measurements $Z_{1:k-1}$ up to time $k-1$ is [CB07]

$$D_{k|k-1}(\mathbf{x}_k|Z_{1:k-1}) = \gamma_k(\mathbf{x}_k) + \int \phi_{k|k-1}(\mathbf{x}_k, \mathbf{x}_{k-1}) D_{k-1|k-1}(\mathbf{x}_{k-1}|Z_{1:k-1}) d\mathbf{x}_{k-1}. \tag{3.9}$$

With the term

$$\phi_{k|k-1}(\mathbf{x}_k, \mathbf{x}_{k-1}) = P_S(\mathbf{x}_{k-1}) f_{k|k-1}(\mathbf{x}_k|\mathbf{x}_{k-1}) + b_{k|k-1}(\mathbf{x}_k|\mathbf{x}_{k-1}). \tag{3.10}$$

Here, $\gamma_k(\cdot)$ denotes the PHD for spontaneous birth at time k, $P_S(\cdot)$ is the probability that the target survives from the previous time step $k-1$ to the current time step k, $f_{k|k-1}(\cdot|\cdot)$ denotes the single-target motion distribution and $b_{k|k-1}(\cdot|\cdot)$ denotes the PHD of a spawned target.

Update Step

The updated posterior PHD $D_{k|k}(\mathbf{x}_k|Z_{1:k})$, which takes the current measurement Z_k into account can be expressed as [CB07]

$$D_{k|k}(\mathbf{x}_k|Z_{1:k}) = \left[\nu(\mathbf{x}_k) + \sum_{\mathbf{z} \in Z_k} \frac{\psi_{k,\mathbf{z}}(\mathbf{x}_k)}{\kappa_k(\mathbf{z}) + \langle D_{k|k-1}, \psi_{k,\mathbf{z}} \rangle} \right] D_{k|k-1}(\mathbf{x}_k|Z_{1:k-1}), \tag{3.11}$$

where

$$\begin{aligned}\nu(\mathbf{x}_k) &= 1 - P_D(\mathbf{x}_k),\\ \psi_{k,\mathbf{z}}(\mathbf{x}_k) &= P_D(\mathbf{x}_k)g(\mathbf{z}|\mathbf{x}_k),\\ \kappa_k(\mathbf{z}) &= \lambda_k u_k(\mathbf{z}).\end{aligned}$$

Here, $P_D(\mathbf{x}_k)$ denotes the probability of detection, $\nu(\mathbf{x}_k)$ denotes the probability of non-detection of state $\mathbf{x}_k$, $g(\mathbf{z}|\mathbf{x}_k)$ is the single target measurement likelihood function, $\kappa_k(\mathbf{z})$ is the intensity of the clutter RFS K_k, λ_k is the Poisson parameter specifying the expected number of false alarms and $u_k(\mathbf{z})$ is the probability density over the state-space of clutter points. $\langle \cdot, \cdot \rangle$ denotes the inner product and is computed as follows

$$\langle D_{k|k-1}, \psi_{k,\mathbf{z}} \rangle = \int D_{k|k-1}(\mathbf{x}_k|Z_{1:k-1})\psi_{k,\mathbf{z}}(\mathbf{x}_k)d\mathbf{x}_k. \tag{3.12}$$

3.3 PHD-Filter Implementations

The PHD-Filter propagates the first moment of the full multi-target posterior in time, which is computationally less complex than propagating the whole multi-target posterior. Approximating the PHD utilizing a sequential Monte Carlo (SMC) approach further reduces the computational complexity. The key idea behind the SMC approach is to represent the required posterior density function by a set of random samples with associated weights and to compute estimates based on these samples and weights [AMGC02]. The implementation of the SMC PHD-Filter adapted from [CB07] is described in Section 3.3.1.

Also a closed-form solution of the PHD-Filter exists and is called the Gaussian mixture (GM) PHD-Filter. It was proposed by [VM05]. The filter assumes the target movement and the targets birth process to follow linear Gaussian dynamics. The means, covariances and weights of the Gaussian mixture components are propagated in time. This is similar to the Kalman filter in the single-target case. The implementation of the GM PHD-Filter is adapted from [VM06] and explained in Section 3.3.2.

3.3.1 Sequential Monte Carlo Implementation

The implementation of the SMC PHD-Filter is adapted from [CB07] and is explained in detail here, supported by pseudo code written in Alg. 1 to Alg. 7. For an introduction on SMC methods for filtering see [AMGC02].

The pseudo code of the SMC PHD-Filter is illustrated in Alg. 1. First, N particles $\mathbf{x}_k^{(i)}$ and their corresponding weights $w_k^{(i)}$ are initialized from a given prior PHD $D_{0|0}$ with $\hat{T}_0$ present targets (Alg. 2). Once this initialization is complete, the iteration over the received measurement sets begins. For each iteration step k, the PHD prediction (Alg. 3), PHD update (Alg. 4) and particle resampling (Alg. 5) steps are performed. Then data association is made where first the targets are extracted from the particle PHD distribution (Alg. 6), and then a labelling of the target tracks (Alg. 7) is performed. In the following the single steps are explained in more detail.

Initialization

In this step, N particles are drawn from an initial PHD $D_{0|0}$. The shape of the initial PHD may be arbitrary. If no knowledge about how the measurements are distributed is present, e.g. a uniform distribution over the whole state-space of the initial particles can be used. This is also the most general case of how the the initial particles are distributed. The pseudo code is illustrated in Alg. 2.

Particle PHD Prediction

This step predicts the PHD, represented by the particles' states and weights. Particles that have survived from the previous time-step, $\left\{w_k^{(i)}, \mathbf{x}_k^{(i)}\right\}_{i=1}^{N_{k-1}}$, are predicted using the single-target motion model (compare with (3.9)). Furthermore, M newborn particles are injected into the system. Like in the initialization step, if no assumption about the target distribution is made the newborn particles are drawn from a uniform density across the whole state-space. The pseudo code is illustrated in Alg. 3.

Particle PHD Update

The update of the particle PHD takes the current measurement set Z_k into account. All predicted particle states $\tilde{\mathbf{x}}_k^{(i)}$ are evaluated against all measurements within the RFS Z_k and reweighted accordingly (compare with (3.11)). Non-detected targets are accounted for by adding the intensity of non-detected targets $\nu(\mathbf{x})$ to the measurements. To filter clutter, which might be present in the measurements, particle weights are influenced by the clutter PHD intensity $\kappa_k(\mathbf{z})$. The result of this step is a set of updated weights for all particles within the system. The updated particle weights approximate the present multi-target PHD. The pseudo code is illustrated in Alg. 4.

Particle Resampling

Like all particle filters which are based on sequential importance sampling, the SMC PHD-Filter suffers from a phenomenon called the degeneracy problem [AMGC02]. After a few iterations, all but a few particles will still have a significant and non-zero weight. To overcome this problem, resampling has to be performed. This can be done if a threshold of a degeneracy measure is exceeded or simply at each time-step. Here, resampling is performed in every time-step. One simple method of resampling is to randomly pick particles based on their likelihood distribution [Sim06]. First, the cummulative distribution function (cdf) is built based on the current particle distribution in state-space. Next, a set of new particles is generated. Therefore, N times the number of estimated targets particles are randomly drawn based on their likelihood described by the cdf. This resampling approach is described in [Sim06]. The pseudo code is illustrated in table Alg. 5.

Target Estimation

Target estimation describes the step of estimating the targets position based on the present particle set representation. A way of extracting the targets, is to estimate the number of present targets in the current time-step, and then use this information to perform k-means clustering [Llo82] on top of it. The number of cluster centres for the k-means algorithm is then set equal to the estimated target number. The drawback of this method is, that if the estimated number of targets is wrong, also the outcome, which are the estimated target states, will be wrong. The pseudo code is illustrated in Alg. 6.

Target Track Labelling

Target track labelling associates the estimated targets $\mathbf{m}_k^{(i)}$, which were estimated in the previous computation step, along multiple time-steps. Target values from the previous time-step $k-1$ are predicted into the current time-step k using the single-target motion distribution. Next, a state-transition likelihood matrix B_k is built based on the target state $\mathbf{m}_k^{(i)}$, the predicted target state $\hat{\mathbf{m}}_{k|k-1}^{(i)}$ and the covariance matrix $S_{k,i}$ of $\mathbf{m}_k^{(i)}$. The pseudo code is illustrated in Alg. 7.

Algorithm 1 SMC PHD-Filter

$\left\{w_0^{(i)}, \mathbf{x}_0^{(i)}\right\}_{i=1}^{N} \leftarrow \text{INITIALIZATION}\left(N, D_{0|0}, \hat{T}_0\right)$ ▷ see Alg. 2
for $k = 1 \dots N_R$ **do**
  $\left\{\tilde{w}_{k|k-1}^{(i)}, \tilde{\mathbf{x}}_k^{(i)}\right\}_{i=1}^{R_k} \leftarrow \text{PREDICTION}\left(\left\{w_k^{(i)}, \mathbf{x}_k^{(i)}\right\}_{i=1}^{N_{k-1}}, M\right)$ ▷ see table Alg. 3
  $\left\{\tilde{w}_k^{(i)}, \tilde{\mathbf{x}}_k^{(i)}\right\}_{i=1}^{R_k} \leftarrow \text{UPDATE}\left(\left\{\tilde{w}_{k|k-1}^{(i)}, \tilde{\mathbf{x}}_k^{(i)}\right\}_{i=1}^{R_k}, Z_k, \lambda_k\right)$ ▷ see Alg. 4
  $\left\{w_k^{(i)}, \mathbf{x}_k^{(i)}\right\}_{i=1}^{N} \leftarrow \text{RESAMPLE}\left(\left\{\tilde{w}_k^{(i)}, \tilde{\mathbf{x}}_k^{(i)}\right\}_{i=1}^{R_k}, N\right)$ ▷ see Alg. 5
  $\left\{\mathbf{m}_k^{(i)}, S_{k,i}\right\}_{i=1}^{K} \leftarrow \text{TARGET ESTIMATION}\left(\left\{w_k^{(i)}, \mathbf{x}_k^{(i)}\right\}_{i=1}^{N_k}\right)$ ▷ see Alg. 6
  if $k \geq 2$ **then**
    target labels $\leftarrow$ TARGET LABELING$\left(\left\{\mathbf{m}_k^{(i)}, S_{k,i}\right\}_{i=1}^{K}, B_{\text{thresh}}\right)$ ▷ see Alg. 7
  end if
end for

Algorithm 2 Initialization step of SMC PHD-Filter

function INITIALIZATION$(N, D_{0|0}, \hat{T}_0)$
  ▷ At time $k = 0$ initialize N particles drawn from the prior PHD $D_{0|0}$
  for $i = 1, \dots, N$ **do**
    sample particle $\mathbf{x}_0^{(i)} \sim D_{0|0}$
    assign initial particle weight $w_0^{(i)} = \frac{\hat{T}_0}{N}$
    ▷ $\hat{T}_0 \dots$ estimated number of targets
  end for
  return $(\left\{w_0^{(i)}, \mathbf{x}_0^{(i)}\right\}_{i=1}^{N})$
end function

Algorithm 3 Prediction step of SMC PHD-Filter

function PREDICTION($\left\{w_k^{(i)}, \mathbf{x}_k^{(i)}\right\}_{i=1}^{N_{k-1}}, M$)
  for $i = 1 \dots N_{k-1}$ **do** ▷ iterate over all survived particles N_{k-1}
    sample $\tilde{\mathbf{x}}_k^{(i)}$ from single-target motion distribution $f_{k|k-1}(\cdot|\mathbf{x}_{k-1}^{(i)})$
    evaluate predicted weights $\tilde{w}_{k|k-1}^{(i)} = P_S(\mathbf{x}_{k-1}^{(i)}) w_{k-1}^{(i)}$
    ▷ $P_S(\cdot) \dots$ probability of survival
  end for
  for $i = N_{k-1} + 1, \dots N_{k-1} + M$ **do** ▷ iterate over all M newborn particles
    sample $\tilde{\mathbf{x}}_k^{(i)}$ from uniform density across state-space
    compute weights of newborn particles $\tilde{w}_{k|k-1}^{(i)} = \frac{\gamma_k(\tilde{\mathbf{x}}_k^{(i)})}{M} = \frac{1}{M}$
    ▷ the PHD for sponaneous birth is set to one $\gamma_k(\cdot) = 1$
  end for
  $R_k = N_{k-1} + M$ ▷ $R_k \dots$ total number of particles
  return ($\left\{\tilde{w}_{k|k-1}^{(i)}, \tilde{\mathbf{x}}_k^{(i)}\right\}_{i=1}^{R_k}$)
end function

Algorithm 4 Update step of SMC PHD-Filter

function UPDATE($\left\{\tilde{w}_{k|k-1}^{(i)}, \tilde{\mathbf{x}}_k^{(i)}\right\}_{i=1}^{R_k}, Z_k, \lambda_k$)
  for each $\mathbf{z} \in Z_k$ **do**
    for $i = 1, \dots, R_k$ **do**
      $\psi_{k,z}^{(i)}(\tilde{\mathbf{x}}_k^{(i)}) = P_D(\tilde{\mathbf{x}}_k^{(i)}) g(\mathbf{z}|\tilde{\mathbf{x}}_k^{(i)})$
      ▷ $P_D(\cdot) \dots$ probability of detection, $g(\cdot|\cdot) \dots$ single-target likelihood function
    end for
    compute inner product $\langle \tilde{w}_{k|k-1}, \psi_{k,\mathbf{z}} \rangle = \sum_{i=1}^{R_k} \psi_{k,\mathbf{z}}^{(i)}(\tilde{\mathbf{x}}_k^{(i)}) \tilde{w}_{k|k-1}^{(i)}$
    compute clutter PHD $\kappa_k(\mathbf{z}) = \lambda_k u_k(\mathbf{z})$ ▷ with $\lambda_k = \lambda$ and $u_k(\mathbf{z}) = 1$ if the measurement is within the state-space
  end for
  for $i = 1, \dots, R_k$ **do**
    compute PHD of non-detected target $\nu(\tilde{\mathbf{x}}_k^{(i)}) = 1 - P_D(\tilde{\mathbf{x}}_k^{(i)})$
    update weights $\tilde{w}_k^{(i)} = \left[\nu(\tilde{\mathbf{x}}_k^{(i)}) + \sum_{\mathbf{z} \in Z_k} \frac{\psi_{k,\mathbf{z}}^{(i)}(\tilde{\mathbf{x}}_k^{(i)})}{\kappa_k(\mathbf{z}) + \langle \tilde{w}_{k|k-1}, \psi_{k,\mathbf{z}} \rangle}\right] \tilde{w}_{k|k-1}^{(i)}$
  end for
  return ($\left\{\tilde{w}_k^{(i)}, \tilde{\mathbf{x}}_k^{(i)}\right\}_{i=1}^{R_k}$)
end function

Algorithm 5 Resample step of SMC PHD-Filter

function RESAMPLE($\left\{\tilde{w}_k^{(i)}, \tilde{\mathbf{x}}_k^{(i)}\right\}_{i=1}^{R_k}, N$)
  estimate number of targets: $\hat{T}_k = \sum_{i=1}^{R_k} \tilde{w}_k^{(i)}$
  compute new number of particles: $N_k = N \cdot \text{round}(\hat{T}_k)$ ▷ round$(\cdot)\ldots$ round to nearest integer
compute cdf:
  $c_1 = \frac{\tilde{w}_k^{(1)}}{\hat{T}_k}$
  for $j = 2, \ldots, R_k$ **do**
    $c_j = c_{j-1} + \frac{\tilde{w}_k^{(j)}}{\hat{T}_k}$
  end for
resample step:
  for $i = 1, \ldots, N_k$ **do**
    pick $r_i \sim U \in [0, 1]$ ▷ draw sample uniform from state-space
    $j = 2$
    while $\sum_{m=1}^{j-1} c_m < r_i$ **do**
      $j = j + 1$
    end while
    $\mathbf{x}_k^{(i)} = \tilde{\mathbf{x}}_k^{(j)}$ ▷ set new particle with index i equal to old particle with index j
    $w_k^{(i)} = \frac{\hat{T}_k}{N}$
  end for
  return $(\left\{w_k^{(i)}, \mathbf{x}_k^{(i)}\right\}_{i=1}^{N_k})$
end function

Algorithm 6 Target estimation using k-means Algorithm

function TARGET ESTIMATION($\left\{w_k^{(i)}, \mathbf{x}_k^{(i)}\right\}_{i=1}^{N_k}$)
perform k-means clustering:
  $K = \text{round}(\sum_{i=1}^{N_k} w_k^{(i)})$ ▷ number of cluster centers
  cluster particles $\left\{\mathbf{x}_k^{(i)}\right\}_{i=1}^{N_k}$ into K cluster sets $\{C_1, \ldots, C_K\}$ with cluster centre $\mathbf{m}_k^{(i)}\Big|_{i=1}^{K}$ according to [Llo82]
  compute cluster covariance $S_{k,i} = \text{cov}(C_i)\ \forall\ K$ clusters ▷ cov$(\cdot)\ldots$ covariance function
  return $\left(\left\{\mathbf{m}_k^{(i)}, S_{k,i}\right\}_{i=1}^{K}\right)$
end function

Algorithm 7 Track association and labelling

function TARGET LABELING($\left\{ \left(\mathbf{m}_k^{(i)}, S_{k,i} \right) \Big|_{i=1}^{K} \right\}_{i=1}^{N_R}, B_{\text{thresh}}$)
  for $j = 1, \ldots, \hat{T}_{k-1}$ **do**
    $\hat{\mathbf{m}}_{k|k-1}^{(j)} = F\mathbf{m}_{k-1}^{(j)}$ ▷ predict new state
  end for
construct state transition likelihood matrix:
  for $j = 1, \ldots, \hat{T}_{k-1}$ **do**
    for $i = 1, \ldots, \hat{T}_k$ **do**
      $B_k(i,j) = exp\left(-\frac{1}{2} \left(\mathbf{m}_k^{(i)} - \hat{\mathbf{m}}_{k|k-1}^{(j)} \right) S_{k,i}^{-1} \left(\mathbf{m}_k^{(i)} - \hat{\mathbf{m}}_{k|k-1}^{(j)} \right)^{\mathrm{T}} \right)$
    end for
  end for
associate target track:
  if $B_k(i,j)$ is maximum $\forall i, j$ **and** $B_k(i,j) > B_{\text{thresh}}$ **then**
    ▷ B_{thresh} ... threshold defining minimum labelling-likelihood
    label target $\mathbf{m}_k^{(i)}$ with label of $\mathbf{m}_{k-1}^{(j)}$
  else
    pick new label for target $\mathbf{m}_k^{(i)}$
  end if
  return target labels
end function

3.3.2 Gaussian Mixture Implementation

The GM PHD-Filter offers a closed form solution of the PHD recursion [VM06]. This requires three additional assumptions:

- Each single target follows a linear Gaussian dynamical model with the state-transition pdf

$$f_{k|k-1}(\mathbf{x}_k|\mathbf{x}_{k-1}) = \mathcal{N}(\mathbf{x}_k; F_{k-1}\mathbf{x}_{k-1}, Q_{k-1}), \tag{3.13}$$

  and the single-target measurement likelihood

$$g_k(\mathbf{z}_k|\mathbf{x}_k) = \mathcal{N}(\mathbf{z}_k; H_k\mathbf{x}_k, R_k). \tag{3.14}$$

  Here, $\mathcal{N}(\cdot; \mathbf{m}, P)$ denotes a Gaussian pdf with mean $\mathbf{m}$ and covariance P. In the state-transition equation, F_{k-1} denotes the state transition matrix and Q_{k-1} is the process noise covariance matrix. The single-target measurement likelihood equation contains the observation matrix H_k and the observation noise covariance R_k.

- The probability of target survival and detection are state independent:

$$P_{S,k}(\mathbf{x}_k) = P_{S,k} \tag{3.15}$$

  and

$$P_{D,k}(\mathbf{x}_k) = P_{D,k}. \tag{3.16}$$

- The intensities of the birth and spawn RFS are Gaussian mixtures of the form

$$\gamma_k(\mathbf{x}_k) = \sum_{i=1}^{J_{\gamma,k}} w_{\gamma,k}^{(i)} \, \mathcal{N}(\mathbf{x}_k; \mathbf{m}_{\gamma,k}^{(i)}, P_{\gamma,k}^{(i)}) \tag{3.17}$$

  and

$$\beta_{k|k-1}(\mathbf{x}_k|\mathbf{x}_{k-1}) = \sum_{i=1}^{J_{\beta,k}} w_{\beta,k}^{(i)} \, \mathcal{N}(\mathbf{x}_k; F_{\beta,k-1}^{(i)}\mathbf{x}_{k-1} + \mathbf{d}_{\beta,k-1}^{(i)}, Q_{\beta,k-1}^{(i)}). \tag{3.18}$$

  Here, the intensity of the birth RFS is a summation of Gaussian intensities with mean $\mathbf{m}_{\gamma,k}^{(i)}$ and covariance $P_{\gamma,k}^{(i)}$. The weight $w_{\gamma,k}^{(i)}$ marks the expected number of newborn targets at $\mathbf{m}_{\gamma,k}^{(i)}$. The Gaussian mixture components of the intensity of spawn RFS have their means at $F_{\beta,k-1}^{(i)}\mathbf{x}_{k-1} + \mathbf{d}_{\beta,k-1}^{(i)}$ and covariances $Q_{\beta,k-1}^{(i)}$. A newly spawned target is assumed to be in the proximity of its parent given by the distance $\mathbf{d}_{\beta,k-1}^{(i)}$. This condition is justified with the example of a target firing, e.g., a missle. The newly spawned target origins at the parents' position and it is detected at a distance $\mathbf{d}_{\beta,k-1}^{(i)}$ from its parent.

For the complete derivation of the GM PHD-Filter the reader is referred to [VM06]. Their implementation has been adapted here and the pseudo code is illustrated in Alg. 8. In the

following, the steps of the algorithm are explained in more detail.

Algorithm 8 GM PHD-Filter

initialization:
set $k = 0$
select $\left\{ w_0^{(i)}, \mathbf{m}_0^{(i)}, P_0^{(i)} \right\}_{i=1}^{J_0}$

iteration:
for $k = 1, \ldots, N_R$ **do**
    $\left(\left\{ w_k^{(i)}, \mathbf{m}_k^{(i)}, P_k^{(i)} \right\}_{i=1}^{J_k} \right) \leftarrow$ GM PHD-FILTER$\left(\left\{ w_{k-1}^{(i)}, \mathbf{m}_{k-1}^{(i)}, P_{k-1}^{(i)} \right\}_{i=1}^{J_{k-1}}, Z_k \right)$
    ▷ pseudocode can be found in table I in [VM06]
pruning:

    $\left(\left\{ w_k^{(j)}, \mathbf{m}_k^{(j)}, P_k^{(j)} \right\}_{j=1}^{J_{k,p}} \right) \leftarrow$ PRUNING$\left(\left\{ w_k^{(i)}, \mathbf{m}_k^{(i)}, P_k^{(i)} \right\}_{i=1}^{J_k} \right)$
    ▷ pseudocode can be found in table II in [VM06]

multi-target state extraction:
    $\left(\left\{ \mathbf{m}_k^{(j)}, P_k^{(j)} \right\}_{j=1}^{K} \right) \leftarrow$ STATE EXTRACTION$\left(\left\{ w_k^{(j)}, \mathbf{m}_k^{(j)}, P_k^{(j)} \right\}_{j=1}^{J_{k,p}} \right)$
    ▷ pseudocode can be found in table III in [VM06]
target labelling:
    if $k \geq 2$ **then**
        target labels $\leftarrow$ TARGET LABELLING$\left(\left\{ \mathbf{m}_k^{(j)}, P_k^{(j)} \right\}_{j=1}^{K}, B_{\text{thresh}} \right)$
        ▷ pseudocode can be found in Alg. 7
    end if
end for

Initialization

In the initialization step, an initial target distribution encoded in the Gaussian mixture components can be set. If no knowledge about the initial target distribution is available, the number of GM components J_0 is set to zero.

Iteration

In each iteration step k a new measurement set Z_k is available. The GM PHD-FILTER$(\cdot)$ function performs the PHD recursion. This function computes the posterior PHD by taking the current measurements and the present targets, which are encoded in a Gaussian mixture representation, into account. The posterior PHD itself is then again represented by a Gaussian mixture distribution. The pseudo code of the GM PHD-FILTER$(\cdot)$ function is not restated here, but it can be found in table I in [VM06].

Pruning

The GM PHD-Filter propagates the GM components in time. With no additional steps, the number of GM components in the posterior PHD of the GM PHD-Filter would grow without bound. At time k, $\mathcal{O}(J_{k-1}|Z_k|)$ Gaussian mixture components are needed [VM06]. Here, J_{k-1} is the number of Gaussian mixtures present at time $k-1$ and $|Z_k|$ is the number of elements in the current measurement set Z_k. To limit the growing number of Gaussian mixture components, a pruning mechanism has to be applied. The pruning algorithm used is given in table II in [VM06]. GM components with a weight smaller than a specified truncation threshold are neglected. GM components which are located within a merging threshold are merged into a single GM component. The weight of this new GM component is the summation of the merged GM components. If the number of GM components is still higher than a maximum value $J_{\max}$, only the $J_{\max}$ GM components with highest weight are reported.

Multi-Target State Extraction

The multi-dimensional mean of a GM component directly represents an estimate of the multi-dimensional state of the target. The height of the peaks of the PHD give the estimate of the number of targets present at the peaks position [PVSD04, Mah03]. The height of the peaks of the PHD is encoded in the weight of the GM component with its mean as the state of the target. The total number of targets $\hat{T}_k$ present at time-step k can be estimated with a summation over all the weights of the GM components in that time-step. The multi-target state estimation is given in table III in [VM06]. For all GM components in the system, targets are only reported if the weight of that component exceeds a threshold, e.g. 0.5. The number of targets reported for a single GM component depend on its weight and is round to the nearest integer value.

Target Track Association and Labelling

Target track association and labelling is equal to the method described in Alg. 7.

4 Multi-target Distance Metrics

In the single target case, well-known performance measures exist. If the true state $\mathbf{x}_k$ of a system in time-step k is known the distance to its estimate $\hat{\mathbf{x}}_k$ can be computed using any distance metric, e.g. the Euclidean distance $d(\mathbf{x}_k, \hat{\mathbf{x}}_k) = \sqrt{(\mathbf{x}_k - \hat{\mathbf{x}}_k)^{\mathrm{T}}(\mathbf{x}_k - \hat{\mathbf{x}}_k)}$. In the multi-target case, the distance between a set of true target states $X_k = \{\mathbf{x}_{k,1}, \mathbf{x}_{k,2} \ldots, \mathbf{x}_{k,N}\}$ and a set of estimated target states $\hat{X}_k = \{\hat{\mathbf{x}}_{k,1}, \hat{\mathbf{x}}_{k,2} \ldots, \hat{\mathbf{x}}_{k,M}\}$ has to be evaluated. This introduces a problem known as the association problem. Which target estimates in $\hat{X}_k$ are associated with which true target states in X_k? Furthermore, if a cardinality miss-match between the the true target state set X_k and the target estimate set $\hat{X}_k$ is present, how is this handled by the distance metric? A multi-target distance metric has to incorporate this. In the following, three known multi-target distance metrics are presented.

4.1 Hausdorff Distance Metric

The Hausdorff distance [HM02], [SVV08] is defined by

$$d_H(X, Y) = \max \left\{ \max_{x \in X} \min_{y \in Y} d(x, y), \max_{y \in Y} \min_{x \in X} d(x, y) \right\}. \tag{4.1}$$

Here, $d_H(X, Y)$ is the Hausdorff distance of the two finite non-empty subsets $X = \{x_1, \ldots, x_m\}$ and $Y = \{y_1, \ldots, y_m\}$ of a finite set W.

Three major drawbacks of this metric are noted in [SVV08],

- it does not consider cardinality errors,
- it penalizes outliers heavily and
- it cannot be reasonably defined if one of the sets is empty.

4.2 Wasserstein Distance Metric

The Wasserstein distance was introduced in [HM02] and is given as

$$d_p(X,Y) = \min_C \left(\sum_{i=1}^{m} \sum_{j=1}^{n} C_{i,j} d(x_i, y_j)^p \right)^{\frac{1}{p}}. \tag{4.2}$$

Here, $d_p(X,Y)$ is the Wasserstein distance of order p of two finite subsets $X = \{x_1, \ldots, x_m\}$ and $Y = \{y_1, \ldots, y_n\}$ of a finite set W. C is a $m \times n$ transportation matrix with the constraint

$$\sum_{j=1}^{n} C_{i,j} = \frac{1}{m} \text{ for } 1 \leq i \leq m \text{ and } \sum_{i=1}^{m} C_{i,j} = \frac{1}{n} \text{ for } 1 \leq j \leq n. \tag{4.3}$$

Furthermore, $\sum_{j=1}^{n} \sum_{i=1}^{m} C_{i,j} = 1$. The transportation matrices form a convex polytope and the computation of the distance $d_p(X,Y)$ is then of minimizing a linear function on a convex domain [HM02].
This metric copes with the problems of the Hausdorff metric, but still has several drawbacks [SVV08]:

- inconsistency of the metric, i.e. the Wasserstein distance depends on how well the elements of the set X are balanced among the set Y,
- contrived construction for differing cardinalities, i.e. individual objects are decomposed into small parts, which makes it hard to interpret the resulting distance from an intuitive point of view,
- geometry dependent behaviour, i.e. the order of magnitude of the Wasserstein distance depends on the geometry of the ground truth,
- undefined if cardinality is zero,
- incompatibility with mathematical theory, such as point process theory.

4.3 OSPA Distance Metric

The optimal sub pattern assignment (OSPA) distance metric is based on the Wasserstein distance metric. It is defined as [SVV08]

$$\bar{d}_p^{(c)} = \left[\frac{1}{n} \min_{\pi \in \Pi_n} \sum_{i=1}^{m} d^{(c)}(x_i, y_{\pi(i)})^p + c^p(n-m) \right]^{\frac{1}{p}}. \tag{4.4}$$

Here, $\bar{d}_p^{(c)}$ is the OSPA distance of the two finite subsets $X = \{x_1, \ldots, x_m\}$ and $Y = \{y_1, \ldots, y_n\}$ of a finite set W. The distance term $d^{(c)}(x,y) = \min(c, d(x,y))$, i.e. an arbitrary distance $d(x,y)$, cut-off at c. Π_n is the set of permutations on $\{1, 2, \ldots, n\}$, p and c are metric parameters, where p describes the order and c is the cut-off value. The parameter p defines how

outliers are treated. A large value of p has the effect of putting more focus on outliers, in the sense that the miss-distance is larger compared to a small p. The cut-off parameter c affects cardinality errors and also defines the maximum search-radius c of the state $x_i \in X$ to look for a state present in $y_i \in Y$.
As the OSPA distance metric fixes most problems associated with the Hausdorff and Wasserstein distance metric, it will be used as a performance measure in Section 5.

4.4 Examples

Four simple examples should illustrate the use of the OSPA distance as a valid performance measure. The examples are plotted in Fig. 4.1. The multi-target miss distances of these examples are given in Tab. 4.1. For distance calculation the ℓ_1-norm is used, i.e. $p = 1$. For the OSPA-metric the cut-off value is set to $c = 2$. In example one, the set Y is empty. In this case, the Hausdorff distance is defined to be infinite, the Wasserstein distance is undefined and the OSPA distance can be computed using (4.4) as $\bar{d}_p^{(c)} = c$. In the second example, no cardinality error is present and the miss-distance equals the ℓ_1-distance for all three distances. In the third example, a cardinality error is present. This cardinality miss-match of the two sets does not affect the Wasserstein distance, which is zero. In the fourth example, the cardinality of the two sets is equal, two elements in Y and X match perfectly and one element in Y shows a large error. Then from an intuitive perspective, this outlier should not be that dominant in the outcome of a multi-target miss-distance if the other elements of the two sets match perfectly. Unfortunately, this is the case with the Hausdorff distance. In contrast to this, the OSPA distance considers the sub-pattern which can be assigned optimally between the two sets X and Y within the cut-off value c. Entries that are not assigned, are penalized with c^p, which means that their contribution can be controlled by the choice of c.

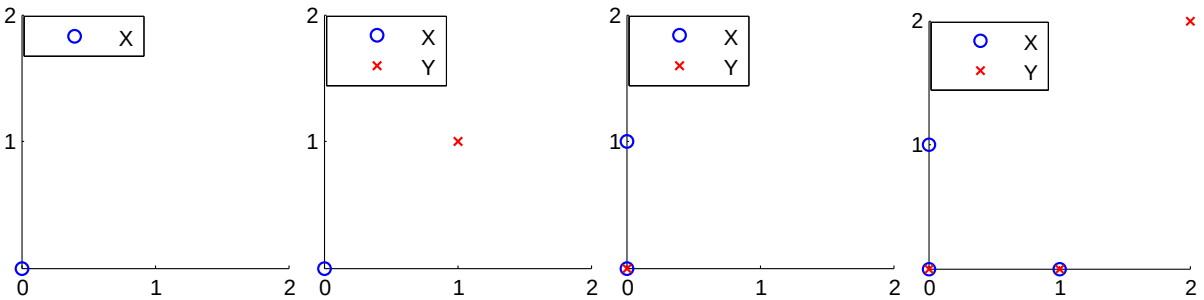

(a) Example 1 (b) Example 2 (c) Example 3 (d) Example 4

Figure 4.1: Multi-target miss-distance examples

Parameter	**Example 1**	**Example 2**	**Example 3**	**Example 4**
$n = \|X\|$	1	1	2	3
$m = \|Y\|$	0	1	1	3
Hausdorff $d_H(X, Y)$	∞	2	1	3
Wasserstein $d_p(X, Y)$	undefined	2	0	1.67
OSPA $\bar{d}_p^{(c)}$	c	2	1	1

Table 4.1: Multi-target miss-distance examples

5 Performance Evaluation

This chapter presents the evaluation of the two PHD-Filter implementations described in Section 3.3. The evaluation was carried out on simulated and real measurement data. The advantages of using simulated measurement data are obvious: The ground truth is perfectly known as well as the clutter model and parameters. Thus, constraints concerning the PHD-Filter and their implementations can be fulfilled. Furthermore, simulated measurement data allow a comparison with a defined ground truth and a performance quality of the filter can be given. Once the implementations are verified in this manner, a field trial with real measurement data can be carried out.

5.1 State-Space Model

Both PHD-Filter implementations use the same constant velocity state-propagation model. A target state $\mathbf{x}_k \in X_k$ is described by four states with the vector

$$\mathbf{x}_k = [\tau, \alpha, \Delta\tau, \Delta\alpha]^{\mathrm{T}}. \tag{5.1}$$

Here, τ denotes the delay and α the amplitude of an MPC. The entries $\Delta\tau, \Delta\alpha$ mark the change of the system state in each time step. The state-space propagation follows the constant velocity model

$$\mathbf{x}_{k+1} = F_k \mathbf{x}_k + \mathbf{v}_k. \tag{5.2}$$

Here, $\mathbf{x}_{k+1}$ is the target state at the time-step $k+1$ with the linear state-update matrix

$$F_k = \begin{bmatrix} 1 & 0 & 1 & 0 \\ 0 & 1 & 0 & 1 \\ 0 & 0 & 1 & 0 \\ 0 & 0 & 0 & 1 \end{bmatrix}. \tag{5.3}$$

The process noise is denoted as $\mathbf{v}_k$. A single measurement $\mathbf{z}_k \in Z_k$ is described by the linear equation

$$\mathbf{z}_k = H_k \mathbf{x}_k + \mathbf{n}_k. \tag{5.4}$$

Here,

$$H_k = \begin{bmatrix} 1 & 0 & 0 & 0 \\ 0 & 1 & 0 & 0 \end{bmatrix} \tag{5.5}$$

is the observation matrix and the vector $\mathbf{n}_k$ denotes the measurement noise. Hence, the measurement consists of τ and α.

5.2 Simulated Measurements

Two types of simulated measurement data are used. One follows the constant-velocity model of the state-space model used in the PHD-Filter implementations. The target movement in the α-τ-plane is therefore linear. For the upcoming discussion this will also be denoted as the linear measurement scenario. The other measurement data follows a non-constant-velocity model and hence violates this linear target dynamics. The target movement in the α-τ-plane is non-linear. This will also be denoted as the non-linear measurement scenario.

5.2.1 Scenario with Linear Motion

The measurement of the constant-velocity scenario is illustrated in Fig. 5.1. The measurement noise $\mathbf{n}_k$ is zero and the ground truth is equal to the measurements. The upper sub-plot contains the amplitude α of the measurement set at each time-step. The lower sub-plot contains the delay τ value of the received measurement. The measurement properties are given in Tab. 5.1. Target movement is restricted to linear dynamics. The number of targets present reaches from three to seven. The cardinality at each time-step is shown in Fig. 5.4(a).

To evaluate the influence of clutter, clutter is added uniformly distributed over the state-space. This is shown in red in Fig. 5.1. The number of clutter values per time-step follows a Poisson distribution with the Poisson parameter $\lambda = 10$.

Performance Results for the SMC PHD-Filter

The SMC PHD-Filter has several parameters which have to be set properly in order to perform well. The parameter setting of the SMC PHD-Filter is given in Tab. 5.2. For each measurement

Parameter	Value	
Measurement set	linear	non-linear
clutter parameter λ	0 or 10	0 or 10
min. number of targets present	3	2
max. number of targets present	7	2
N_R	50	50
$\alpha_{\min}$	0	0.5
$\alpha_{\max}$	1	1
$\Delta\alpha_{\min}$	0	0.01
$\Delta\alpha_{\max}$	0.077	0.01
$\tau_{\min}$	0	0.07
$\tau_{\max}$	1	0.935
$\Delta\tau_{\min}$	0	0.071
$\Delta\tau_{\max}$	0.008	0.071

Table 5.1: Properties of simulated measurements

set, a reasonable trade-off between accuracy and execution time was made. The probability of detection $P_D = 1$, because there are no missed measurements in the measurement set. In the clutter-free scenario the parameter κ_k specifying the intensity of the clutter RFS is set to zero. Each target is represented by a number N_0 of particles. In each time-step, a number of M newborn particles are introduced into the system. The particle variances depend on the measurement set used. The target labelling likelihood is set for good labelling output performance.

Performance results of the SMC PHD-Filter are plotted in Fig. 5.2. The linear clutter-free measurements are plotted in blue in Fig. 5.1. They have been used as measurement inputs to the filter. The variance of the particles in the amplitude domain (upper plot in Fig. 5.2) is higher compared to the delay domain (lower plot). Note that both α and τ domain are normalized to the range $[0, 1]$. The higher variance of the particle in one dimension is due to the properties of the measurement set, where $\Delta\alpha_{\max} > \Delta\tau_{\max}$, which is a situation we also expect for the real measurements. To give the SMC PHD-Filter the ability to follow the target tracks, these filter parameters have to be set at least equal to the true ones. The influence of a larger particle variance σ_α^2 and $\sigma_{\Delta\alpha}^2$ in the amplitude domain compared to a lower particle variance σ_τ^2 and $\sigma_{\Delta\tau}^2$ in the delay domain is directly observable in the plots in Fig. 5.2(a) and Fig. 5.2(b). In Fig. 5.2(a) the particle variance around a state value is large, whereas in Fig. 5.2(b) it is small. In the case where the particle variance is high, also the estimated target states after k-means clustering will have a higher variance around the real targets.

As described in Section 3.3.1, the targets are extracted from the particle representation using k-means clustering. The outcome of this clustering step is plotted in Fig. 5.2 and Fig. 5.3. In the latter, the k-means outcome is plotted against the ground truth. The k-means outcome agrees well with the ground truth. In the case where no clutter is present in the measurement set the ground truth equals the measurement set. For some time-steps, e.g. $k = 7$ and $k = 9$, the estimated target state in one dimension is not in the proximity of its ground truth. This is

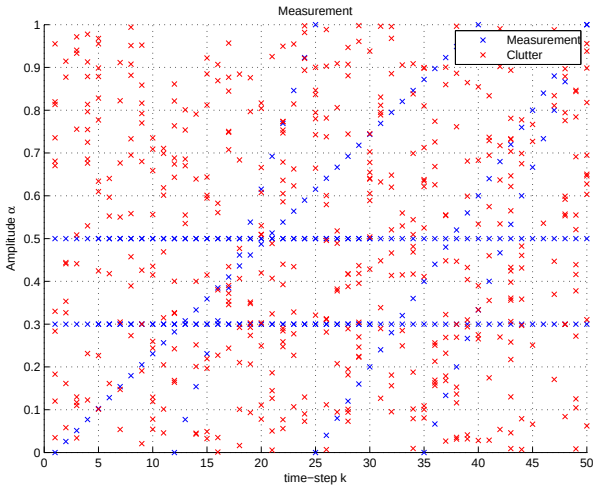

(a) Amplitude α

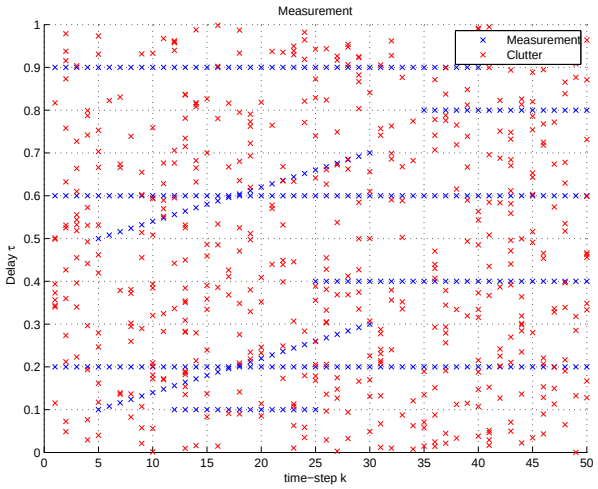

(b) Delay τ

Figure 5.1: Simulated measurements: linear case; clutter present with an average of $\lambda = 10$ spurious measurements per time-step

caused by the k-means clustering algorithm, where the initial cluster centres are selected randomly from the present particles. If the initially selected cluster centres are chosen from the same particle mass, the k-means algorithm can produce two closely spaced cluster centres as long as the global optimization criterion is fulfilled. Also, if an initially selected cluster centre is based on a particle outlier the k-means algorithm can output that particle state as the optimal cluster centre. The reported cluster centre is then not located in the location of the particle masses. This is a specific issue of the k-means clustering algorithm. The estimated cardinality of the SMC PHD-Filter and the true cardinality are plot in Fig. 5.4(a). Because no clutter is present and no measurements are missing, the estimated cardinality matches with the real one. In the first iteration step, the estimated cardinality is zero, because up to then no particles are in the system yet. Then, for the next time-step M new particles have been injected into the system and the cardinality is fully encoded in the particles weight. The multi-target miss-distances averaged over 100 Monte-Carlo runs are plotted in Fig. 5.5. The cut-off parameter for the OSPA

Parameter	**Value**			
Measurement set	linear	linear	non-linear	non-linear
clutter parameter λ	0	10	0	10
Filter setting				
P_S	0.95	0.995	0.95	0.995
P_D	1	1	1	1
κ_k	0	1/50	0	1/200
N_0	500	200	100	500
M	500	500	20	1000
Measurement-target likelihood variance:				
$\sigma^2_{\alpha,\mathrm{L}}$	$3 \cdot 10^{-2}$	$3 \cdot 10^{-2}$	$1 \cdot 10^{-2}$	$1 \cdot 10^{-2}$
$\sigma^2_{\tau,\mathrm{L}}$	$3 \cdot 10^{-3}$	$3 \cdot 10^{-3}$	$5 \cdot 10^{-3}$	$5 \cdot 10^{-3}$
Particle birth variance:				
$\sigma^2_{\alpha,\mathrm{b}}$	1	1	1	1
$\sigma^2_{\tau,\mathrm{b}}$	1	1	1	1
$\sigma^2_{\Delta\alpha,\mathrm{b}}$	$1 \cdot 10^{-1}$	$1 \cdot 10^{-1}$	$1 \cdot 10^{-2}$	$1 \cdot 10^{-2}$
$\sigma^2_{\Delta\tau,\mathrm{b}}$	$1 \cdot 10^{-2}$	$1 \cdot 10^{-2}$	$5 \cdot 10^{-2}$	$5 \cdot 10^{-2}$
Process noise variance:				
$\sigma^2_{\alpha,\mathbf{n}}$	0	0	0	0
$\sigma^2_{\tau,\mathbf{n}}$	0	0	0	0
$\sigma^2_{\Delta\alpha,\mathbf{n}}$	$5 \cdot 10^{-2}$	$5 \cdot 10^{-2}$	$5 \cdot 10^{-3}$	$5 \cdot 10^{-3}$
$\sigma^2_{\Delta\tau,\mathbf{n}}$	$5 \cdot 10^{-3}$	$5 \cdot 10^{-3}$	$2 \cdot 10^{-2}$	$2 \cdot 10^{-2}$
Association threshold:				
B_{thresh}	$1 \cdot 10^{-1}$	$1 \cdot 10^{-3}$	$1 \cdot 10^{-3}$	$6 \cdot 10^{-1}$

Table 5.2: Parameter setting of SMC PHD-Filter for simulated measurement sets

distance was set to $c = 0.1$ and order $p = 2$. The OSPA miss-distance shows maxima at the time-steps where the cardinality of the ground truth changes, because the distance between the estimated and the true target position is high (compare with Fig. 5.3). If a target appears or disappears in the state-space, the estimated multi-target posterior pdf represented by the PHD is no longer valid and particles drawn from it reside at invalid target positions. Therefore, the distance between the estimated target position and the true target position is high at this time-step.

The labelled result using the clutter-free linear measurement set is plotted in Fig. 5.6(a). The association threshold for target track labelling was set to $B_{\mathrm{thresh}} = 0.1$. The choice of B_{thresh} is a trade-off between maintaining target track continuity and suppressing association of different estimated target states to the same target track. A small value of B_{thresh} associates neighbouring target states with the same target track, whereas a large value of B_{thresh} prevents this. An increased B_{thresh} leads to a higher number of not associated targets and shorter target tracks. This threshold depends on the input measurement set of the SMC PHD-Filter and has to be adjusted by the user to meet the design criteria. Here, the focus was set on target track continuity. In the case where the delay τ stays constant, estimated targets with the same τ are associated to the same track despite the fact that a target state is missing. Then the target track is labelled

with a new label. If the target tracks cross in the state-space the succeeding target is associated to the track with the highest labelling-likelihood. This can cause target tracks with the same label after the crossing. The computation of the labelling-likelihood is outlined in Alg. 7.

In the case where clutter is present in the measurement set (see Fig. 5.1), it is tricky for the SMC PHD-Filter to estimate the correct number of targets. In Fig. 5.4(b), the estimated and the true cardinality are shown. In the first time-steps the estimated cardinality lags behind the true one. Furthermore, it does not stay constant in cases where the true cardinality remains constant. Nevertheless, the estimated cardinality is close to the true cardinality and fluctuates around the true value. An incorrect estimation of the target cardinality is crucial for the target estimation step using k-means clustering. If the number of cluster centres is set too low, particles from different targets will be clustered together, which results in an erroneously estimated target position. On the other hand, if it is set too high, more targets than actually present will be extracted. The first case is worse, because two closely spaced targets are combined into a single one. The second case when the number of cluster centres is set too high, can lead to the behaviour where one target is represented by two closely spaced cluster centres, or to the case where a cluster centre is placed at the position of particles caused by clutter, which has not been filtered by the SMC PHD-Filter. The result of the SMC PHD-Filter for cluttered data is plotted in Fig. 5.7.

In cases where the SMC PHD-Filter does not properly filter out clutter from the measurements, particles will be placed at the position of the measurements caused by them. These particles can cause a problem in the initialization step of the k-means clustering algorithm as previously explained. The OSPA multi-target miss distance, averaged over 100 Monte-Carlo trials, is shown in Fig. 5.5(b). Compared to the clutter-free scenario shown in Fig. 5.5(a) the overall miss-distance has increased. At the time-steps where the cardinality of the ground truth changes, a higher miss-distance compared to the other time-steps is still notable. The miss-distance has significantly increased in the first time-step because the estimated cardinality lags behind the true one (compare with Fig. 5.4(b)).

The labelled results using the cluttered linear measurement set are plotted in Fig. 5.6(b). To optimize the track association and labelling step described in Alg. 7 of the SMC PHD-Filter, the computation of the labelling likelihood should not only consider target states propagated from the previous time-step into the current time-step. A more sophisticated labelling algorithm has to take the evolution of target tracks from the further past into account.

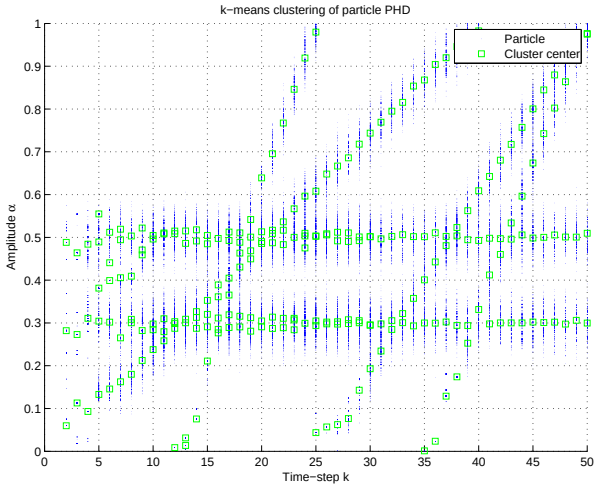

(a) Amplitude α

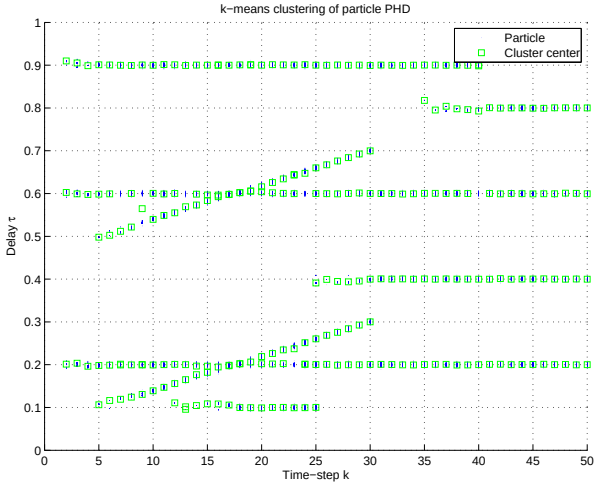

(b) Delay τ

Figure 5.2: SMC PHD-Filter: Outcome of k-means clustering; Measurement set: linear, no clutter present $\lambda = 0$

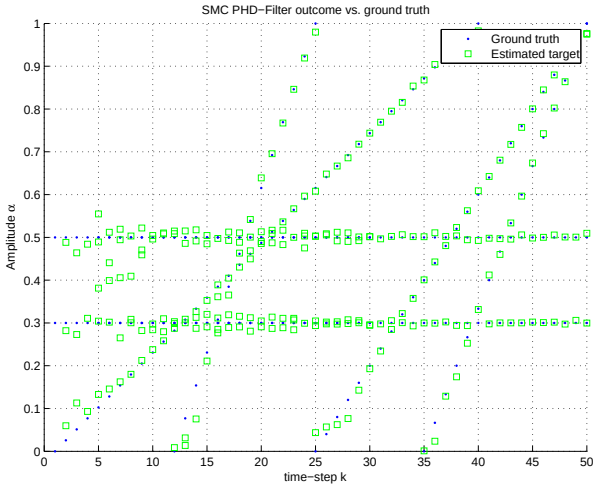

(a) Amplitude α

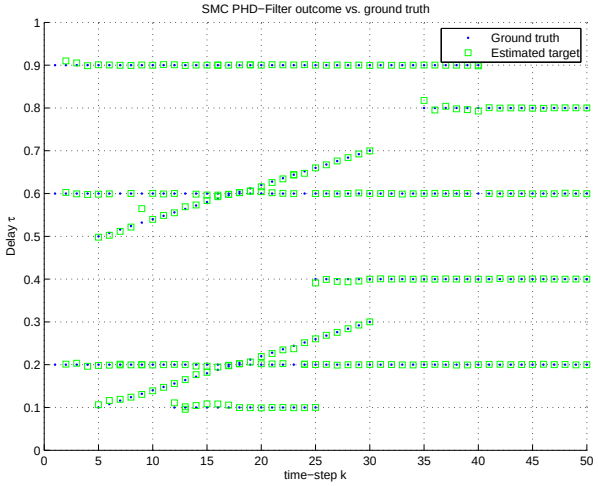

(b) Delay τ

Figure 5.3: SMC PHD-Filter: Ground truth vs. outcome of k-means clustering; Measurement set: linear, no clutter present $\lambda = 0$

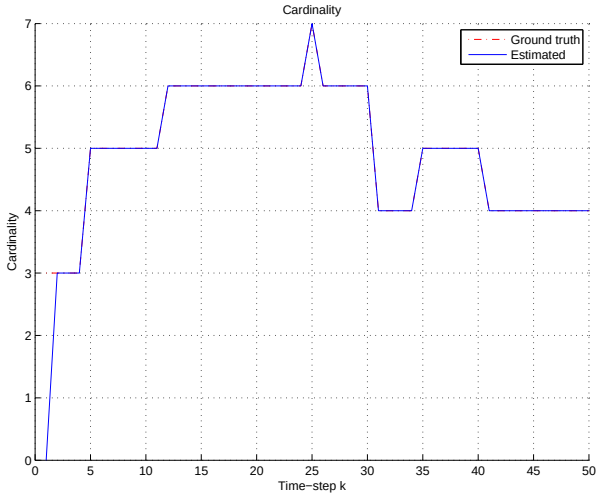

(a) no clutter present $\lambda = 0$

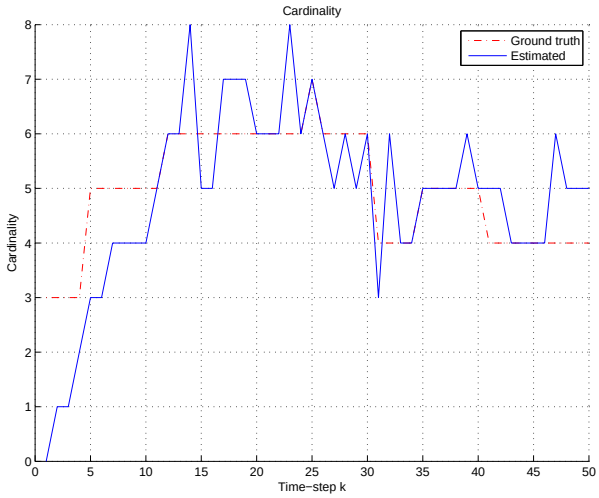

(b) clutter present, $\lambda = 10$

Figure 5.4: SMC PHD-Filter: Estimated vs. true cardinality; Measurement set: linear

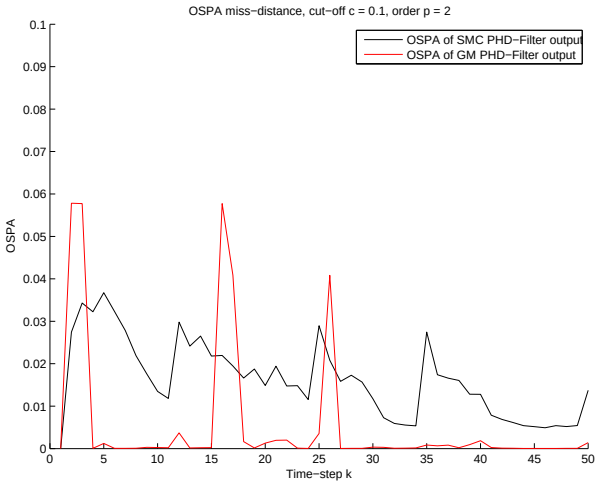

(a) no clutter present $\lambda = 0$

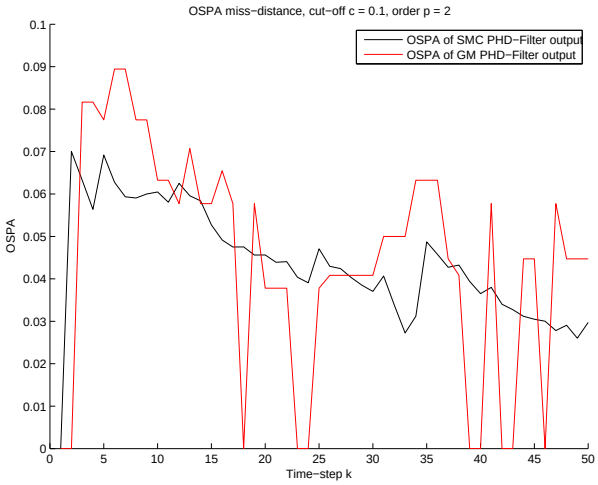

(b) clutter present, $\lambda = 10$

Figure 5.5: OSPA multi-target miss-distances of simulated measurements with the constant velocity model. The miss-distance of the SMC PHD-Filter output was averaged over 100 Monte-Carlo runs.

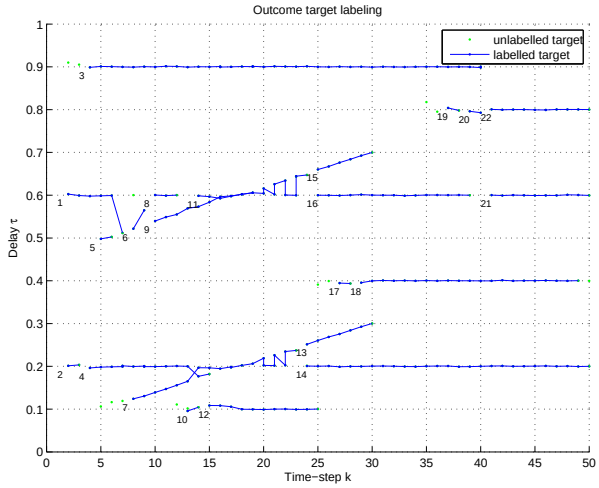

(a) no clutter present, $\lambda = 0$

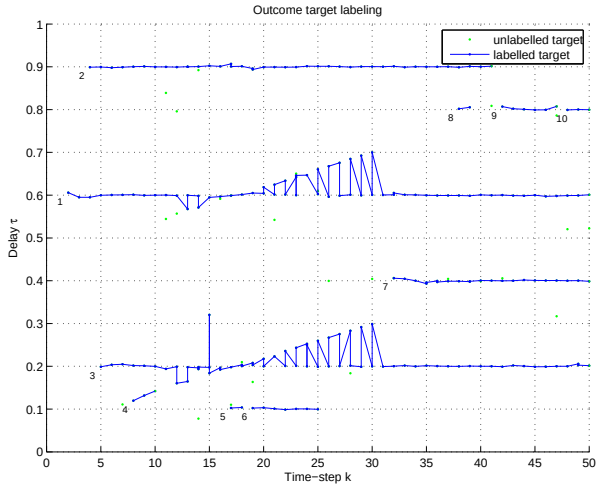

(b) clutter present with $\lambda = 10$

Figure 5.6: SMC PHD-Filter: Labelled outcome; Measurement set: linear

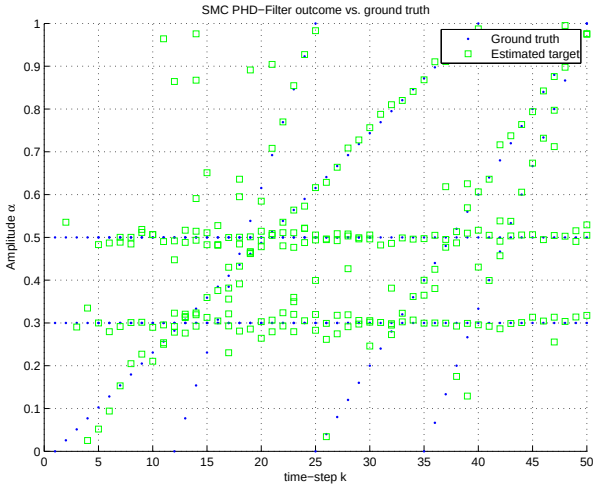

(a) Amplitude α

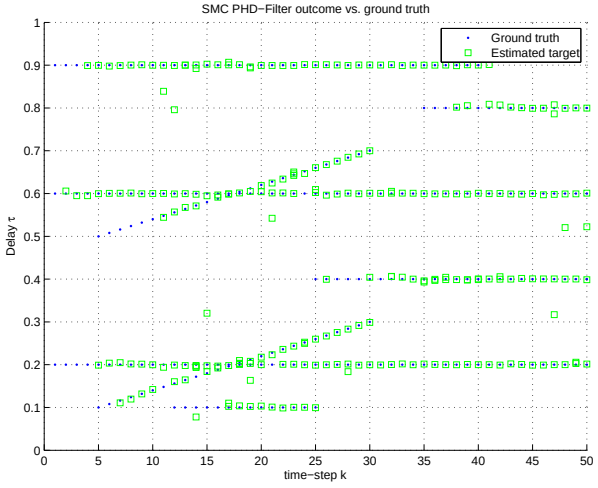

(b) Delay τ

Figure 5.7: SMC PHD-Filter: Ground truth vs. outcome of k-means clustering; Measurement set: linear, clutter present with $\lambda = 10$

Performance Results for the GM PHD-Filter

The parameter setting of the GM PHD-Filter for the different simulated measurement sets is given in Tab. 5.3. The result of the GM PHD-Filter for the linear clutter-free measurement set is shown in Fig. 5.8. Almost all targets have been identified and match well with the ground truth. At the birth of a target, the distance of the estimated target positions and the ground truth is larger compared to succeeding estimates. This is due to the distribution of the birth RFS, which is a Gaussian mixture modelling (GMM). Because we assume that we have no prior knowledge of where the targets will appear in the state-space, a number of GM components is placed equally spaced over the whole state-space. If a new target appears in the state-space, which causes a corresponding measurement in the current measurement set it is evaluated against the birth RFS. The estimated target position is therefore attracted by the position of the closest GM component of the birth distribution. Despite this deviation of the targets birth, the GM PHD-Filter performs better compared to the SMC PHD-Filter. This is also reflected in the OSPA multi-target miss distance plotted in Fig. 5.5(a). In the multi-target state extraction step in Alg. 8, a valid target is extracted only if the weight of a single GM component exceeds the threshold of 0.5. If this is not the case, no target is extracted. This threshold procedure can lead to missed targets in the results of the GM PHD-Filter at time-steps where the weight of a single GM component has lowered due to the update of the current PHD. In Fig. 5.8, such situations of missed targets are observable in some rare time instances. In the previous time-step the target is estimated correctly, then in the current time-step it is missing, because of a lowered weight. In the next time-step, the weight of the GM component has again increased above the threshold and a target state is extracted from it. The estimated cardinality is shown in Fig. 5.10(a) and matches exactly with the ground truth although not all targets have been extracted at each time-step. The summation of the weight of all GM components yields the current targets present. It is reasonable to say that such a hard threshold in the target extraction step in Alg. 8 might not be the optimal choice.

The result of the GM PHD-Filter applied to the linear cluttered measurement set is plotted in Fig. 5.9. The estimated cardinality is shown in Fig. 5.10(b) and is close to the true target cardinality. In the first few time-steps, the estimated cardinality of the GM PHD-Filter lags behind the true one. This could be combated if prior knowledge of the targets birth is incorporated. The GM components of the target birth RFS are placed close to the position in the state-space where the targets will likely appear. If a measurement is situated far away from the birth GM components centres, the likelihood between them is low and the weight of the GM component representing that target state is very small. Additional measurements in succeeding time-steps are needed to push the GM components weight high enough such that a state will be reported at the output of the GM PHD-Filter.

In Fig. 5.9(b), target estimates caused by clutter are observable, which means that the GM PHD-Filter was not able to successfully filter all clutter. This depends on the choice of the parameter value of the clutter intensity κ_k. If κ_k is high, the weight increase of the GM components

in the proximity of received measurements will be low. More measurements from succeeding time-steps are needed until a target is reported. Therefore, also clutter suppression is high. On the other hand, if κ_k is low, the sensitivity to clutter increases, i.e. the filter reacts faster to system changes like a change in cardinality. Hence, clutter suppression is deteriorated.

The OSPA miss-distance is plotted in Fig. 5.5(b). In the first time steps the estimated cardinality lags behind the cardinality of the ground truth. In this case the OSPA miss-distance is close to the cut-off value $c = 0.1$. In the succeeding time steps it decreases, because the estimated cardinality is close to the true cardinality. Compared with the clutter-free scenario, the OSPA miss-distance is relatively large, which is due to some estimated targets caused by clutter. The performance of the GM implementation of the PHD-Filter is worse compared to the SMC implementation plot in Fig. 5.5(b).

Concerning track continuity, the GM implementation of the PHD-Filter is comparable to the SMC implementation. Track continuity of the GM PHD-Filter is plotted in Fig. 5.11. The labelling algorithm used can fail if the targets intersect, because only the previous target state is used for the computation of the target likelihood matrix (see Alg. 8). An increased labelling-threshold can relax this behaviour to some degree, but also will lead to more not associated targets and therefore shorter target tracks.

Parameter	**Value**			
Measurement set	linear	linear	non-linear	non-linear
λ	0	10	0	10
Filter setting:				
P_S	0.9	0.9	0.9	0.9
P_D	1	1	1	1
κ	0	10	0	10
Process noise covariance:				
$\sigma^2_{\tau,\mathrm{Q}}$	$1 \cdot 10^{-3}$	$1 \cdot 10^{-5}$	$1 \cdot 10^{-5}$	$1 \cdot 10^{-5}$
$\sigma^2_{\alpha,\mathrm{Q}}$	$1 \cdot 10^{-3}$	$1 \cdot 10^{-5}$	$1 \cdot 10^{-5}$	$1 \cdot 10^{-5}$
$\sigma^2_{\Delta\tau,\mathrm{Q}}$	$8 \cdot 10^{-2}$	$5 \cdot 10^{-4}$	$5 \cdot 10^{-4}$	$5 \cdot 10^{-4}$
$\sigma^2_{\Delta\alpha,\mathrm{Q}}$	$1 \cdot 10^{-2}$	$5 \cdot 10^{-4}$	$5 \cdot 10^{-4}$	$5 \cdot 10^{-4}$
Measurement noise covariance:				
$\sigma^2_{\tau,\mathrm{R}}$	$1 \cdot 10^{-4}$	$1 \cdot 10^{-6}$	$1 \cdot 10^{-6}$	$1 \cdot 10^{-6}$
$\sigma^2_{\alpha,\mathrm{R}}$	$1 \cdot 10^{-4}$	$1 \cdot 10^{-6}$	$1 \cdot 10^{-6}$	$1 \cdot 10^{-6}$
Birth RFS intensity:				
$\sigma^2_{\tau,\mathrm{B}}$	$1 \cdot 10^{-3}$	$1 \cdot 10^{-5}$	$1 \cdot 10^{-5}$	$1 \cdot 10^{-5}$
$\sigma^2_{\alpha,\mathrm{B}}$	$1 \cdot 10^{-3}$	$1 \cdot 10^{-5}$	$1 \cdot 10^{-5}$	$1 \cdot 10^{-5}$
$\sigma^2_{\Delta\tau,\mathrm{B}}$	$2 \cdot 10^{-2}$	$3 \cdot 10^{-2}$	$3 \cdot 10^{-2}$	$3 \cdot 10^{-2}$
$\sigma^2_{\Delta\alpha,\mathrm{B}}$	$2 \cdot 10^{-2}$	$3 \cdot 10^{-2}$	$3 \cdot 10^{-2}$	$3 \cdot 10^{-2}$
No. of GM components	9	400	9	400
Single GM component weight	1/9	1/400	1/9	1/400
Association threshold:				
B_{thresh}	$1 \cdot 10^{-3}$	$1 \cdot 10^{-3}$	$1 \cdot 10^{-3}$	$1 \cdot 10^{-3}$

Table 5.3: Parameter setting of GM PHD-Filter for simulated measurement sets

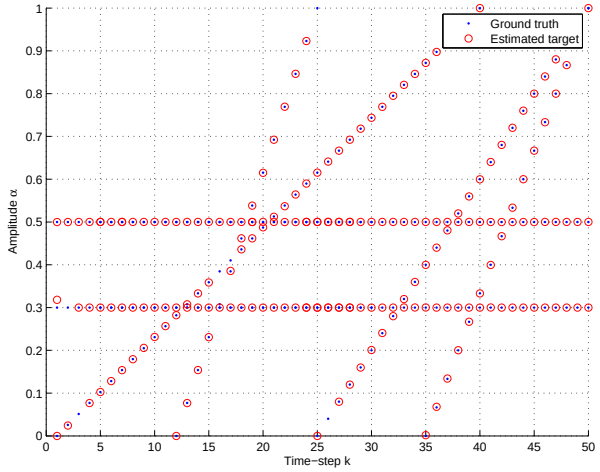

(a) Amplitude α

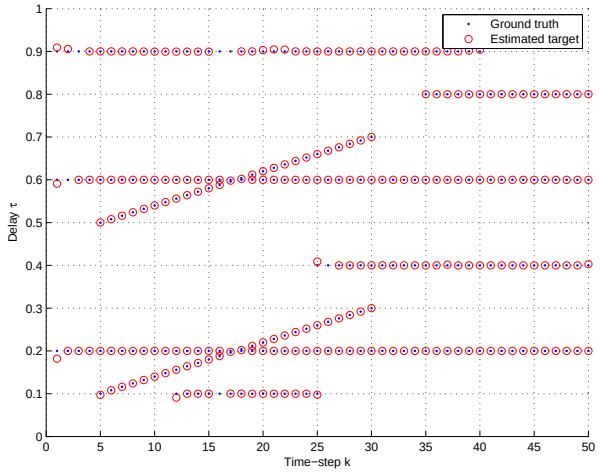

(b) Delay τ

Figure 5.8: Outcome GM PHD-Filter; Measurement set: linear, no clutter present $\lambda = 0$

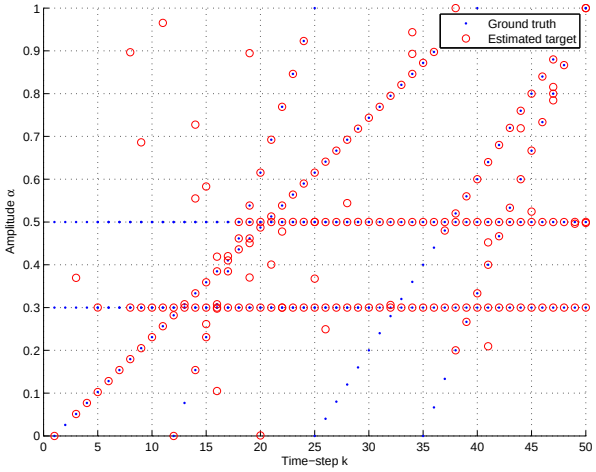

(a) Amplitude α

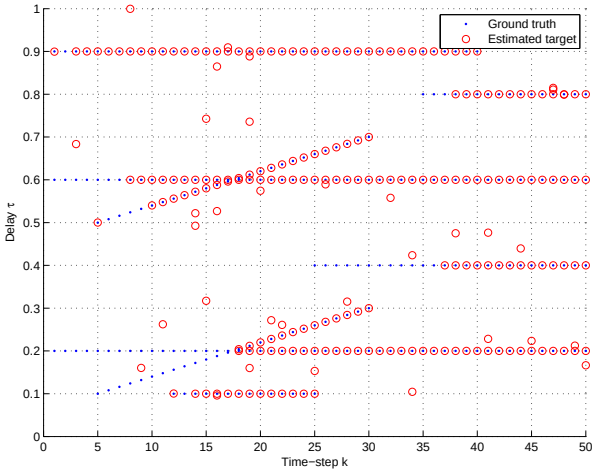

(b) Delay τ

Figure 5.9: Outcome GM PHD-Filter; Measurement set: linear, clutter present $\lambda = 10$

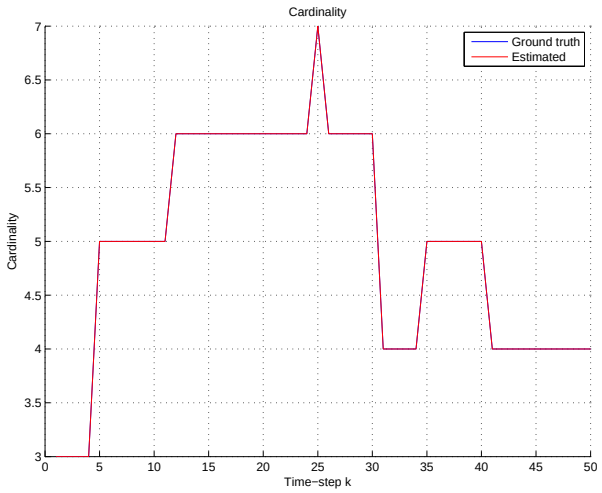

(a) no clutter present $\lambda = 0$

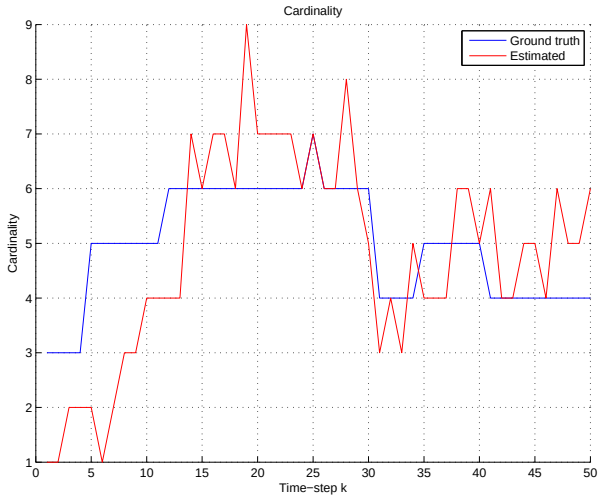

(b) clutter present, $\lambda = 10$

Figure 5.10: Estimated cardinality of GM PHD-Filter; Measurement set: linear

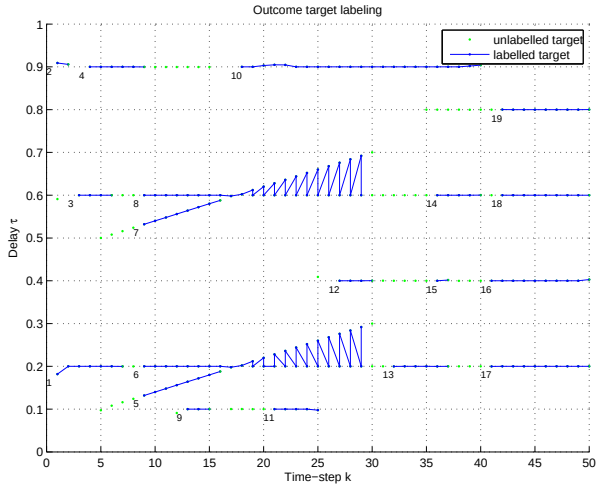

(a) no clutter present $\lambda = 0$

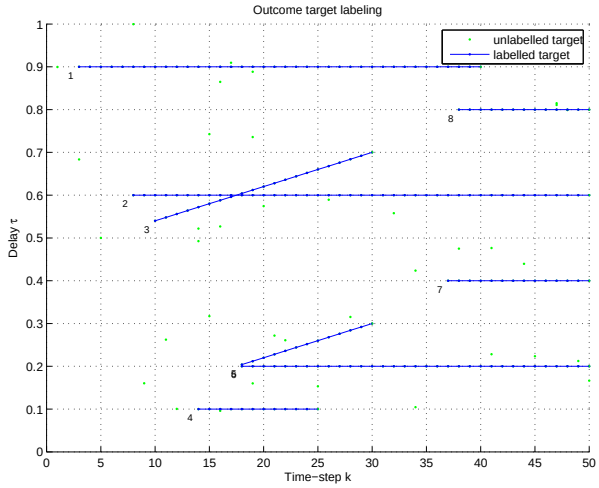

(b) clutter present, $\lambda = 10$

Figure 5.11: Labelled outcome of GM PHD-Filter; Measurement set: linear

5.2.2 Scenario with Non-linear Motion

The clutter-free non-linear motion scenario of the simulated measurement set is plotted in blue in Fig. 5.12. In the upper plot, the amplitude α of the received measurement at each time-step is plot. The lower sub-figure contains the delay τ of the received measurement. The scenario properties are given in Tab. 5.1. The target movement is linear in the amplitude domain and non-linear in the delay domain. The number of targets present is kept constant at a value of two. There is an intersection of both target tracks in time-step $k = 1$ and $k = 37$.

Superimposing uniformly distributed clutter over the whole state-space yields the non-linear measurement set given in Fig. 5.12. The number of clutter values at each time-step follows a Poisson distribution with the Poisson parameter $\lambda = 10$.

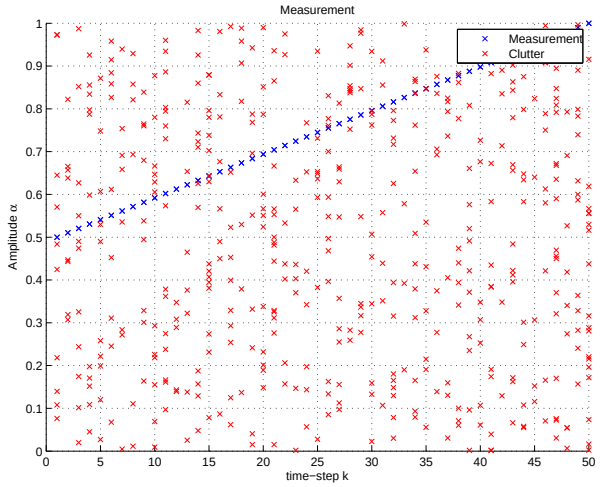

(a) Measured amplitude α

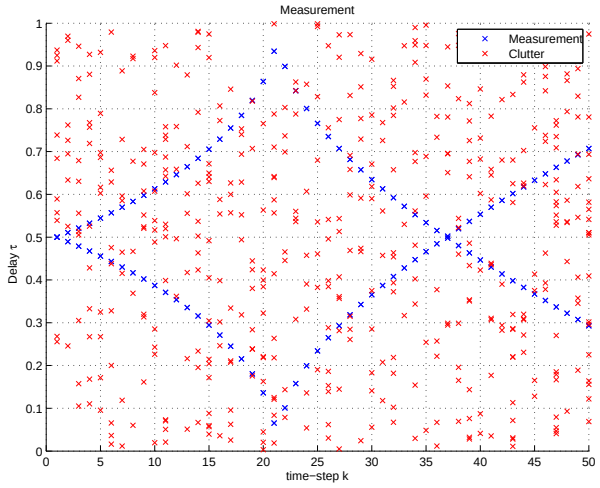

(b) Measured delay τ

Figure 5.12: Simulated measurements: non-linear case, clutter present with $\lambda = 10$

Performance Results for the SMC PHD-Filter

The parameter setting of the SMC PHD-Filter for the non-linear measurement set is given in Tab. 5.2. In the same manner as with the linear measurement set the choice of parameters for the SMC PHD-Filter is optimized to the measurement set and a reasonable trade-off between accuracy and execution time has been made. The state-space model for the SMC PHD-Filter still stays linear and tracking of non-linear moving targets becomes harder. To cope with this inaccuracy, the number of particles per object has to be increased. Then, together with the process noise, particles will survive the update step and a target state can be extracted. This only works for non-linearities where the model miss-match is not too severe. The number of particles per object is $N_0 = 100$ in the clutter-free scenario and $N_0 = 500$ in the case where clutter is present. The number of newborn particles per time-step is $M = 20$ in the clutter-free scenario, compared to $M = 1000$ in the measurement scenario superimposed by clutter.

The outcome of the SMC PHD-Filter for the clutter-free non-linear scenario is plotted in Fig. 5.13. The target states of the linearly changing amplitude parameter in Fig. 5.13(a) and the non-linearly changing delay parameter in Fig. 5.13(b) are estimated quite well until the direction of motion in the τ-dimension changes at time-step $k = 21$. Then, due to the model miss-match and a still too low process noise variance, the SMC PHD-Filter estimates the new target states to follow the same direction in the delay domain as in the time-step before. This results in a wrong target state estimation. After a few more time-steps, the non-linear motion in the delay domain better follows the constant-velocity model and the target estimation error therefore decreases. This behaviour can be observed in the OSPA multi-target miss distance plotted in Fig. 5.16(a).

The OSPA distance shows a maximum at time-step $k = 23$ where the distance between the estimated targets and the ground truth is maximal. Another maximum is at time-step $k = 3$. Since time-step $k = 1$, the two targets have drifted away from each other, but still the SMC PHD-Filter only has followed one target properly. The cardinality is, due to the clutter-free scenario, correctly estimated as two targets (see Fig. 5.15). In the first two time-steps the filter follows only one target and estimates two targets at the same position. In the succeeding time-steps the other target track is found as well, and the OSPA distance decreases as soon as the target estimate is in the vicinity of the ground truth.

The labelled result of the SMC PHD-Filter for the clutter-free measurement set is plotted in Fig. 5.17(a). Target track labelling only works well if the target evolution is nearly linear (approximately time-step $k = 35$ till $k = 50$). Then also the OSPA multi-target miss distance is small (see Fig. 5.16(a)). In the case where the OSPA distance is large, also the result of the target labelling step is unsatisfactory. This can be easily explained, because if the estimated target is not present or somewhere in the state-space but far away from the previous targets, no track association to previous target tracks is possible.

If the non-linear measurement set is superimposed by clutter, target estimation becomes more difficult for the SMC PHD-Filter. The result is plotted in Fig. 5.14. One can observe the higher number of outliers of the estimated k-mean cluster centres compared to the clutter-free measurement scenario plotted in Fig. 5.13. If the SMC PHD-Filter is not able to filter all clutter properly from the measurements, the resulting PHD will be non-zero at the corresponding positions. Particles drawn from the posterior pdf given by the PHD will then also be located at the position of the cluttered measurement. The k-means clustering algorithm randomly selects the initial cluster centres from all particles in the state-space. This can lead to isolated target estimates with only a small amount of underlying particles, which has already been addressed in Section 5.2.1. In Fig. 5.14, estimated target states obviously caused by clutter are visible.

The cardinality is plotted in Fig. 5.15(b), where one can observe the over-/under-estimation of the present target cardinality. The estimated cardinality stays in the vicinity of the ground truth. This, although a high number of measurements caused by clutter are present in the measurements. In time-step $k = 3$, the filter is capable of following one target track (see Fig. 5.14). After additional two time-steps the filter has also found the second target track. Besides the fact that the cardinality is over-estimated for certain time-steps until time-step $k = 21$ the filter follows consequently the two target tracks. In time-step $k = 21$ the delay parameter of the true target states changes its direction of movement and the filter needs a few time-steps (until time-step $k = 25$) to re-find at first one target track and in the succeeding time-steps the second target track. The OSPA multi-target distance penalizes these target mismatches and shows its maxima at these time-steps, which is illustrated in Fig. 5.16(b).

The labelled result of the SMC PHD-Filter using the cluttered non-linear measurement set is plotted in Fig. 5.17(b). Only at time-steps where the OSPA multi-target miss distance is low, track association works well. The outcome is comparable with the clutter-free measurement set. Target tracks are interrupted if the target state is not detected. The succeeding target track then gets assigned a new label.

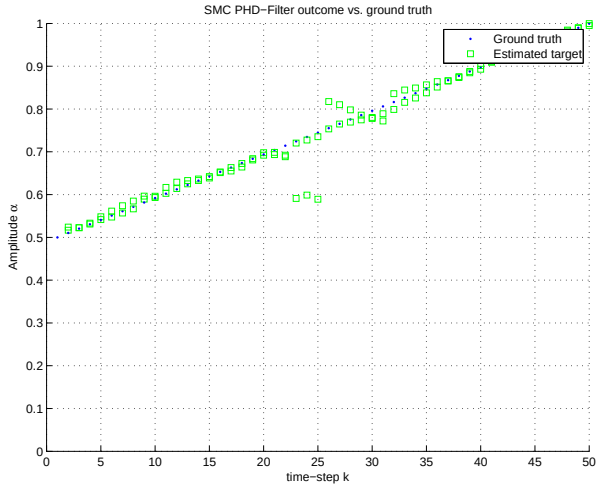

(a) left side

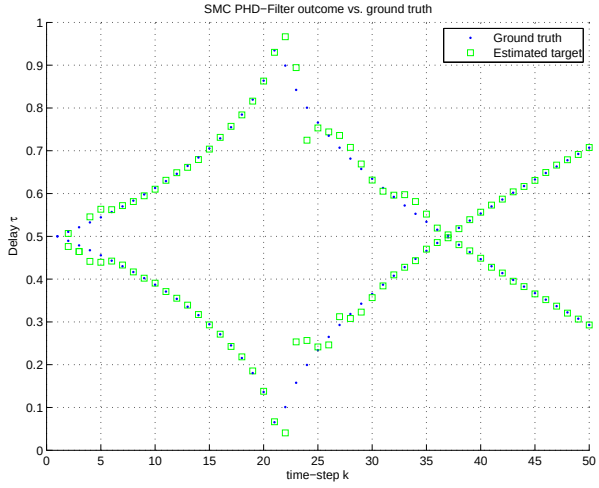

(b) right side

Figure 5.13: SMC PHD-Filter: Ground truth vs. outcome of k-means clustering; Measurement set: non-linear, no clutter present $\lambda = 0$

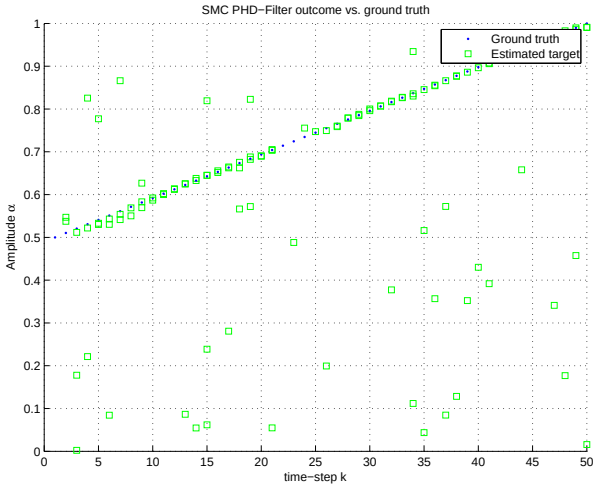

(a) left side

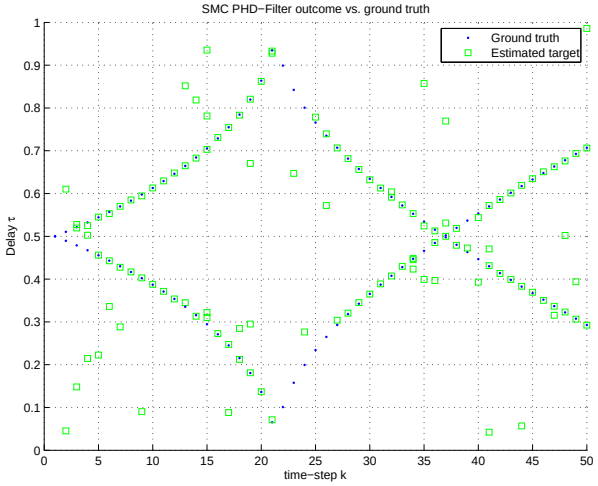

(b) right side

Figure 5.14: SMC PHD-Filter: Ground truth vs. outcome of k-means clustering; Measurement set: non-linear, no clutter present $\lambda = 10$

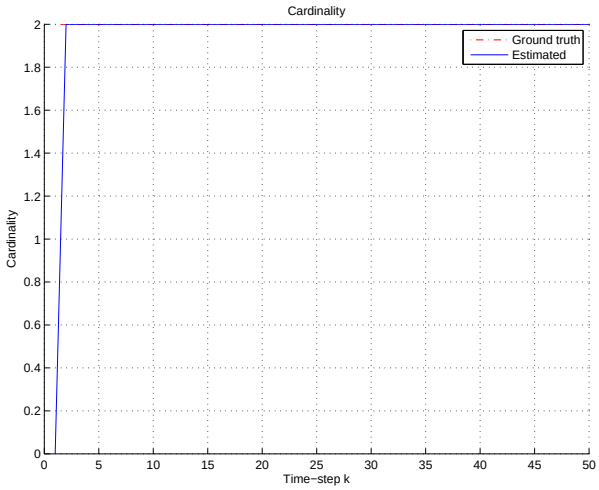

(a) no clutter present $\lambda = 0$

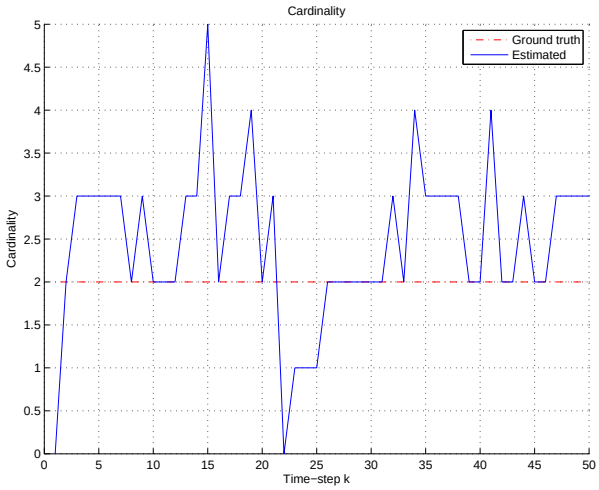

(b) clutter present, $\lambda = 10$

Figure 5.15: SMC PHD-Filter: Estimated vs. true cardinality; Measurement set: non-linear

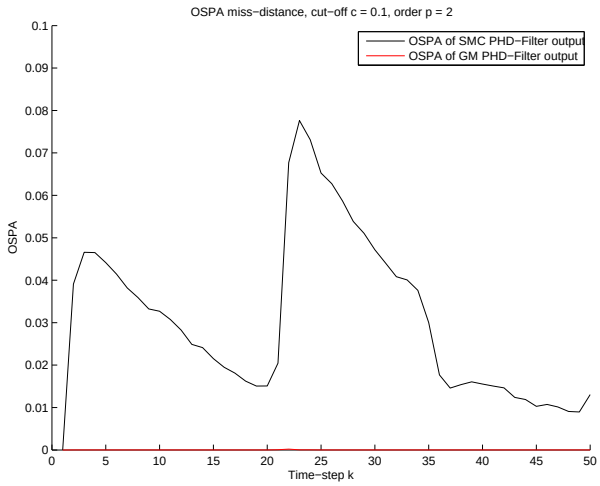

(a) no clutter present $\lambda = 0$

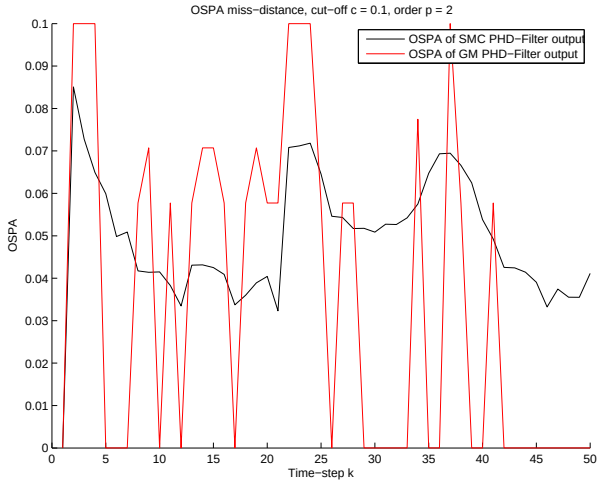

(b) clutter present, $\lambda = 10$

Figure 5.16: OSPA multi-target miss-distances of simulated measurements with the non-constant velocity model. The miss-distance of the SMC PHD-Filter output was averaged over 100 Monte-Carlo runs.

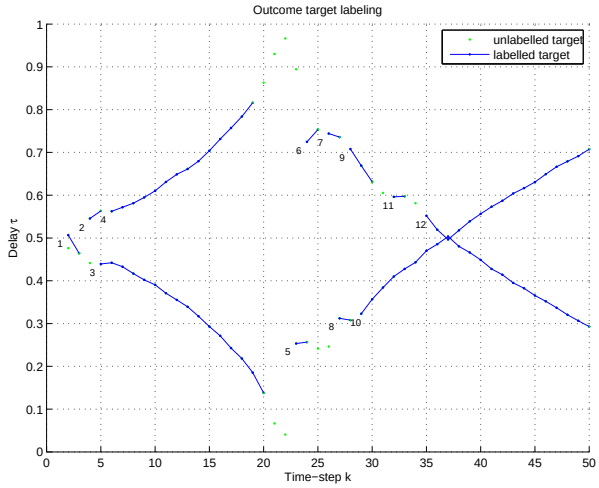

(a) no clutter present, $\lambda = 0$

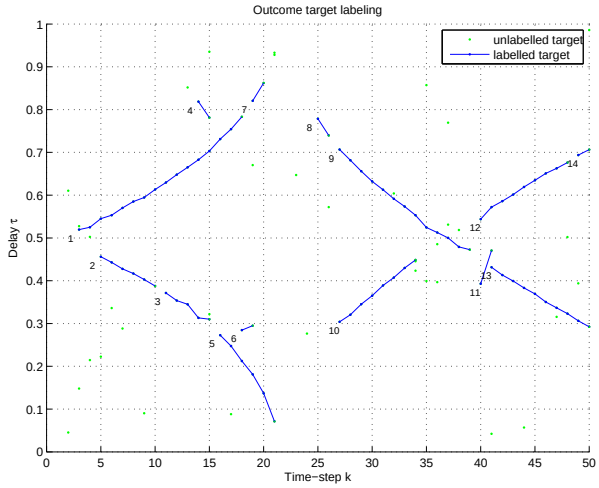

(b) clutter present with $\lambda = 10$

Figure 5.17: SMC PHD-Filter: Labelled outcome; Measurement set: non-linear

Performance Results for the GM PHD-Filter

The parameter setting of the GM PHD-Filter using the non-linear measurement set is shown in Tab. 5.3. The result for the clutter-free non-linear measurement set is plotted in Fig. 5.18. The estimated target states match perfectly with the ground truth. This is supported by the cardinality plot in Fig. 5.20(a) and the all-zero multi-target OSPA miss distance in Fig. 5.16(a). Although the GM PHD-Filter uses a constant velocity model it performs better on this non-constant velocity scenario compared to the constant case. In the linear measurement scenario a deviation between the target estimate and the ground truth was present at the time-step of the targets birth (see Fig. 5.8). Here, this behaviour is not observable, because the distribution of the birth RFS has exactly a GM component placed at the targets birth location by coincidence. In the linear measurement scenario, some target states had not been extracted properly, because no weight of the underlying GM components in the corresponding time-step exceeded the state-extraction threshold of 0.5. In this non-linear measurement scenario, this is not an issue, because the weight of the GM components representing a target state is high from the first time-step on and no target birth lowers the weight of the single GM components. All target states are extracted properly.

The result of the GM PHD-Filter for the non-linear measurement set superimposed by clutter is plotted in Fig. 5.19. The clutter is not entirely successfully filtered out by the GM PHD-Filter, which manifests itself as estimated targets in the output. The estimated cardinality is plotted in Fig. 5.20(b). Only in the beginning (until time-step $k = 3$) and after the time-step where the direction of the true targets delay τ has changed (time-step $k = 21$), the cardinality is under-estimated. In the first case, this is because the distribution of the birth RFS is not exactly located at the real targets birth and therefore the weight increase is too slow. Note, the parameters of the birth RFS are different for the clutter-free and the cluttered non-linear measurement set (see Tab. 5.3). In the second case, the direction of movement of delay τ has changed and the likelihood of the measurements with respect to the propagated GM components leads to a weight decay of the respective GM components. Because of some erroneously detected clutter points, the real target states are not extracted until time-step $k = 25$. Then the weights of the GM components have increased enough, such that the estimated cardinality reached two (see Fig. 5.20(b)) and the outcome of the GM PHD-Filter matches again with the real target states.

The OSPA multi-target miss distance is plotted in Fig. 5.16(b). Whenever the estimated cardinality and the estimated target states match with the ground truth, the OSPA distance is zero, which implies that the detected targets are estimated accurately. Clutter has been successfully filtered out from the measurements by the GM PHD-Filter. An over-estimation in cardinality is penalized with an increase of the OSPA miss-distance. The miss-distance is equal to the cut-off limit of $c = 0.1$ in cases where the true target sate could not be estimated and only pure clutter is present at the filter output (time-step $k = 22$ to $k = 24$).

The labelled output of the GM PHD-Filter applied to the non-linear measurement set is plotted in Fig. 5.21. In both cases the clutter-free and the cluttered environment the target track is well maintained if the target propagation resembles a constant-velocity model. Depending on the value of the labelling-likelihood threshold B_{thresh}, more or less target states are included in the target track where the target movement is strongly non-constant (in the proximity of time-step $k = 21$). If the threshold B_{thresh} is set too, clutter which has not been successfully filtered out by the GM PHD-Filter is associated with the closest target track. Therefore, a compromise in setting the threshold B_{thresh} has to be made. A comparison of the labelled GM PHD-Filter output compared to the SMC implementation (see Fig. 5.17) leads to the conclusion that target track continuity is superior with the method that is used with the GM PHD-Filter. This although the OSPA miss-distance is higher for certain time-steps and reaches the cut-off value $c = 0.1$ compared to the result of the SMC PHD-Filter. Target track life-time is longer compared to the target tracks produced by the SMC PHD-Filter implementation. Intersecting target tracks are assigned to the correct track, because the variance of the estimated target states of the underlying GM components is smaller compared to the estimated target states obtained with the SMC implementation of the PHD-Filter.

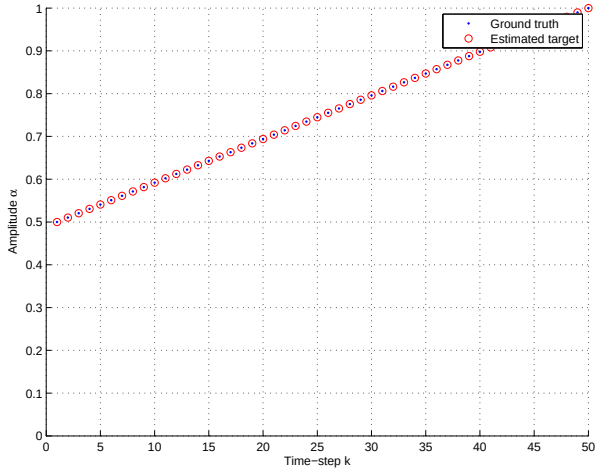

(a) Amplitude α

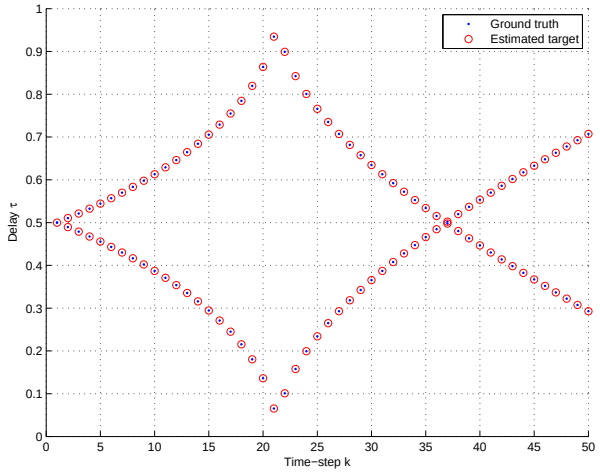

(b) Delay τ

Figure 5.18: Outcome GM PHD-Filter; Measurement set: non-linear, no clutter present $\lambda = 0$

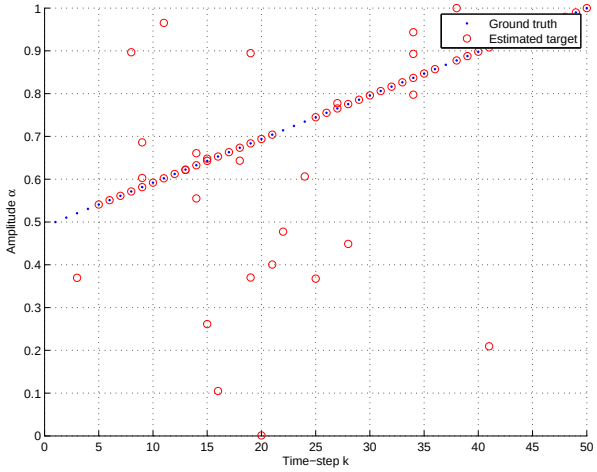

(a) Amplitude α

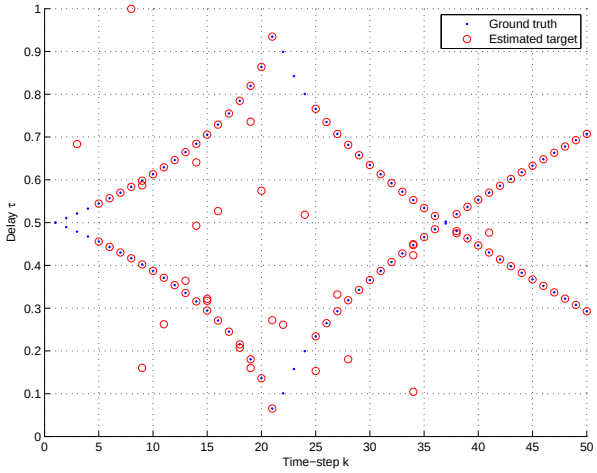

(b) Delay τ

Figure 5.19: Outcome GM PHD-Filter; Measurement set: non-linear, clutter present $\lambda = 10$

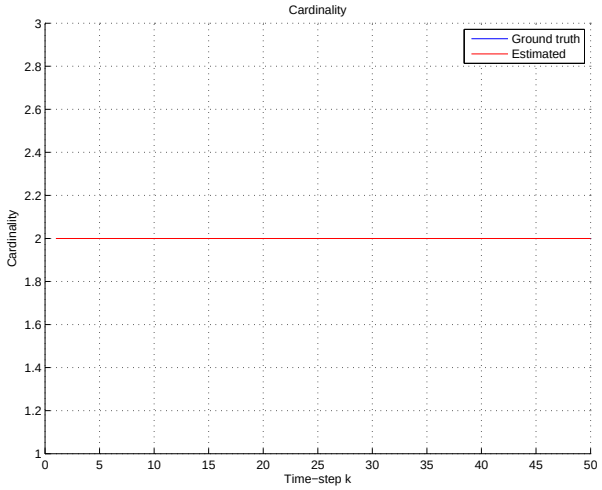

(a) no clutter present $\lambda = 0$

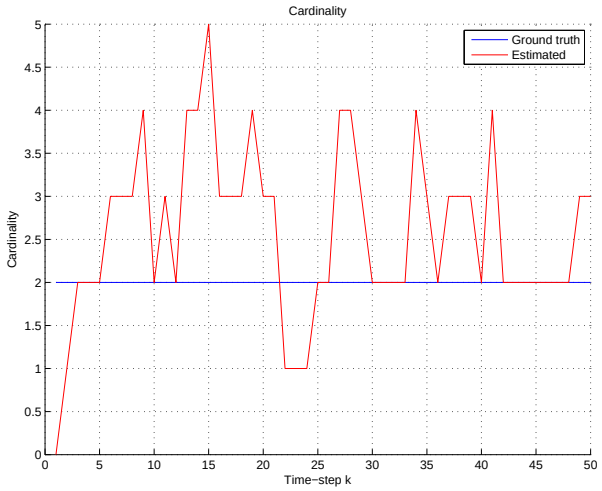

(b) clutter present, $\lambda = 10$

Figure 5.20: Estimated cardinality of GM PHD-Filter; Measurement set: non-linear

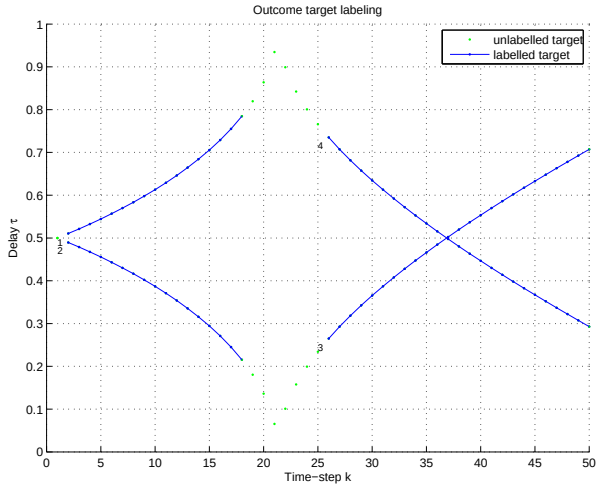

(a) no clutter present $\lambda = 0$

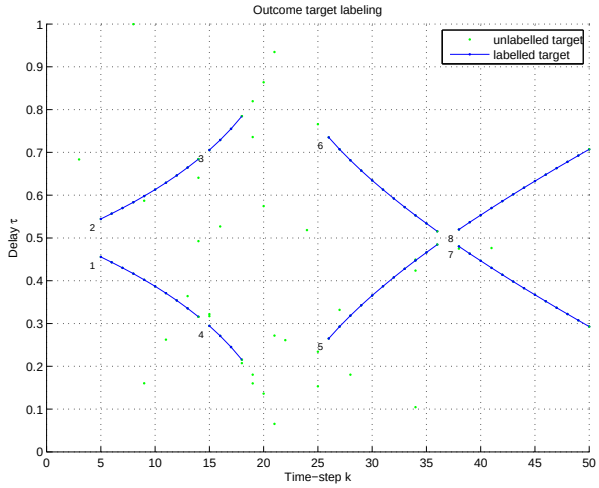

(b) clutter present, $\lambda = 10$

Figure 5.21: Labelled outcome of GM PHD-Filter; Measurement set: non-linear

5.2.3 Summary

The SMC implementation of the PHD-Filter does not impose any restrictions on the target dynamics. In scenarios with approximately constant-velocity the linear state-space model of target movement together with an increased process noise suffices to estimate target states correctly. Whenever this is not the case, non-linear target dynamic can be incorporated in the state-space model of the SMC PHD-Filter. Also, targets may appear anywhere in the state-space. Because the SMC PHD-Filter does not provide a closed-form solution of the PHD recursion, many particles are needed for a good approximation of the posterior PHD. This leads to an increase in execution time. The PHD-Filter itself does not produce estimated targets directly. They have to be extracted from the estimated PHD given by the particle population, by additional clustering. In the SMC PHD-Filter, the k-means clustering algorithm used can introduce new errors. If the estimated cardinality of the SMC PHD-Filter is incorrect, the extracted targets of the clustering algorithm will also differ from the ground truth. This leads to a weak performance of the labelling procedure, because mean and covariance of the estimated targets vary from time-step to time-step and only short target tracks are produced. As the SMC PHD-Filter only approximates the posterior PHD, the estimated targets never exactly match the ground truth and a residual position error is always present. Therefore, the OSPA multi-target miss-distance is low, but non-zero even if no clutter is present in the measurements.

In contrast to the SMC implementation of the PHD-Filter, the GM implementation provides a closed-form solution of the PHD recursion. The PHD can be propagated in time if the single targets follow linear Gaussian dynamics, which is of course a strong assumption. Additionally, the targets birth intensities have to follow a GMM. The restrictions of the GM implementation of the PHD-Filter limit the field of application. If there is a miss-match in target dynamics, the GM PHD-Filter can still be used even though the performance degrades. If target appearance does not match with the given GMM birth distribution, targets will be hardly detected. Using equally spaced GM components over the whole state-space does not lead to a better performance. In cases where the restrictions of the GM implementation are full-filled, the GM implementation is superior to the SMC implementation. Extraction of the targets state is easily done, because the GM components directly represent the targets mean and covariance. Furthermore, because target dynamic is restricted, also the output target tracks of the labelling procedure are very continuous.

5.3 Real Measurements

Here, the performance of the two different PHD-Filter implementations on real measurement data is evaluated. The measurement data used was obtained in an indoor measurement campaign explained in Section 1.4 [FMGW11]. As the measurement are UWB-CIRs, a preprocessing step is needed to convert them to measurement inputs for the PHD-Filters with states α and τ. The preprocessing step is explained first, followed by the results of the PHD-Filter implementations. The properties of the input measurement set are given in Tab. 5.4.

5.3.1 Data Preprocessing

Peak extraction

In the preprocessing step, MPC amplitude estimates are extracted as peaks in the CIRs at each MS position. At first the CIRs are computed with a IDFT of the measured complex channel transfer functions. Next, amplitude peaks, which lie above a given threshold, are extracted from the CIRs with a *search-and-subtract* approach. This is done in an iterative manner: The highest amplitude peak above a suitable threshold is estimated and then subtracted either in frequency [FMGW11] or in time domain [MAGW11] until no more peaks are found, or a certain maximum number of estimated peaks is reached. Here, the latter criterion is used. To subtract a peak in time-domain, the impulse response of the windowing function used in the computation of the IDFT is scaled with the peak amplitude value and then subtracted from the CIR. The cleaned CIR is then used to estimate the next amplitude peak. The peak amplitude threshold is set to 10% of the maximum peak amplitude in the current CIR. A maximum number of 20 peaks is estimated for each CIR. As an example, Fig. 5.22 contains a plot of the CIR at MS position $k = 70$ together with the estimated peaks above the threshold A_k. In Fig. 5.23 the extracted peaks for all MS positions are plot in amplitude and delay domain.

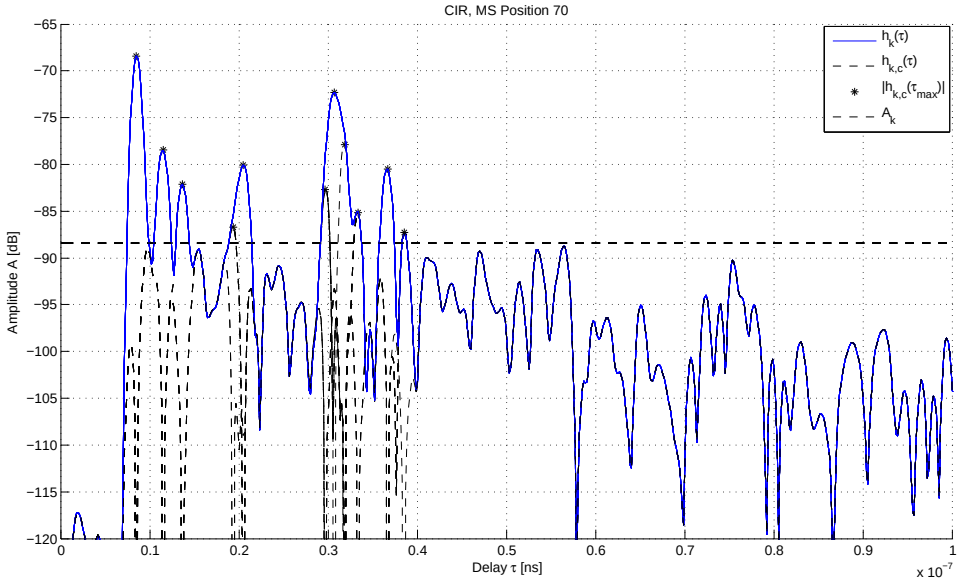

Figure 5.22: Extracted amplitude peaks from CIR at MS position 70

Normalization

The next step is the normalization of the extracted peaks from all the CIRs in the amplitude and delay domain. The peaks are normalized to one, based on the minimum and maximum amplitude and delay values within the measurement set. The normalized measurement set is then used as input for the PHD-Filter. Normalization of the input data set is important in order to make use of the whole state-space of the PHD-Filter, which is then defined between zero and one in the amplitude and delay domain. Also, normalization is needed to avoid different scales for τ and α domain when calculating the miss-distances. The PHD for spontaneous birth was assumed to be uniformly distributed over the whole state-space in the SMC implementation of the PHD-Filter. In the case of the GM implementation, the GM components of the intensity of the birth PHD are placed equally spaced over the whole state-space. Note, the estimated target states of the PHD-Filters are de-normalized and then again normalized to one with the minimum and maximum values of both sets, the estimated target set and the ground truth set. This is needed for calculating the miss-distances. Also the ground truth data set is normalized to one in the amplitude and delay domain based on the overall minimum and maximum values. The ground truth is then used to evaluate the performance of the PHD-Filters outcome.

Ground truth

To obtain an approximate ground truth for the indoor measurements, knowledge about the floor plan is needed. This method is explained in detail in [MAGW11]. The ground truth is plotted in Fig. 5.24. In the plot the LOS component corresponds to the path of measurements having the highest amplitude α and the lowest delay τ. Also, the variation in α is limited for succeeding measurements. MPCs does not show this property. Although, the variation of τ is limited for succeeding measurements, α is strongly fluctuating. Estimating the ground truth out of the measurement set given in Fig. 5.23 will be a challenging task for the PHD-Filters with their constant-velocity model.

Parameter	**Value**
Measurement set:	
Min. amplitude α [dB]	-119
Max. amplitude α [dB]	-66
Min. delay τ [ns]	0
Max. delay τ [ns]	266
Min. number of measurements	5
Max. number of measurements	20
Ground truth:	
Min. cardinality	0
Max. cardinality	10
$\alpha_{\mathrm{dB,min}}$	-114dB
$\alpha_{\mathrm{dB,max}}$	-66dB
Delay τ_{min}	8ns
Delay τ_{max}	173ns

Table 5.4: Measurement properties

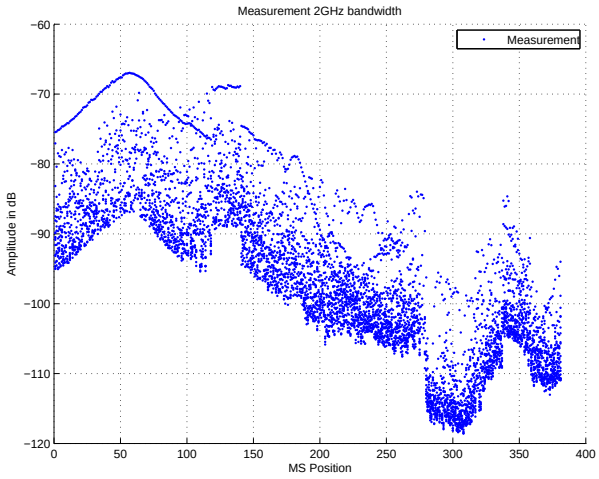

(a) Amplitude α

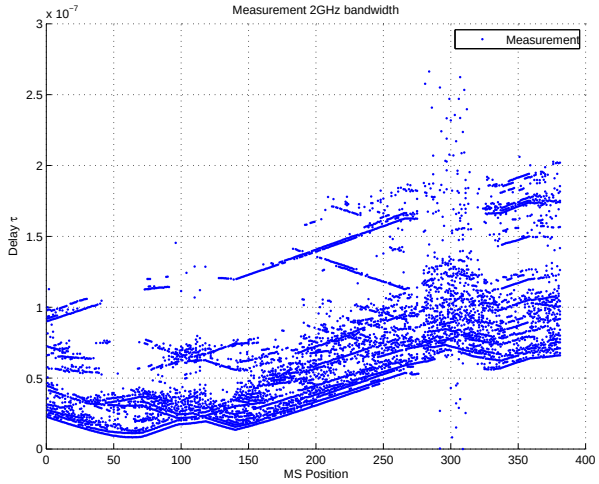

(b) Delay τ

Figure 5.23: Extracted peaks from real measurements

5.3.2 Performance Results for the SMC PHD-Filter

The input measurement set, which contains the extracted and normalized peaks from the measurements, is used as a measurement input to the SMC PHD-Filter. The parameter setting of the filter is given in Tab. 5.5. It has been chosen to be able to track targets whose measurement values do not change rapidly in time, which allows to suppress most of the clutter present. The particles together with the estimated cluster centres of the k-means algorithm are plotted in Fig. 5.25. The SMC PHD-Filter is able to successfully estimate target tracks in cases where the target movement is within the given parameter setting and where the SNR ratio is sufficiently high. In the case of the LOS component, these conditions are fulfilled up to MS position of approximately $k = 120$. The target states are very well estimated. The clutter model used in the PHD-Filter assumes the clutter to be uniformly distributed in the whole state-space and the number of measurements caused by clutter is Poisson distributed with the constant value of λ for all time-steps. Obviously these assumptions are violated here:

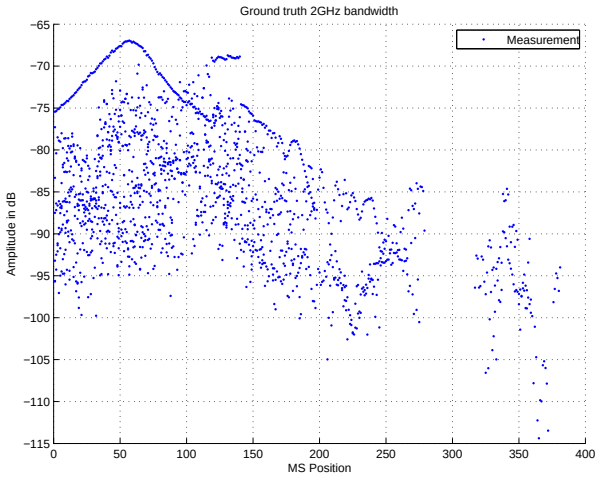

(a) Amplitude α

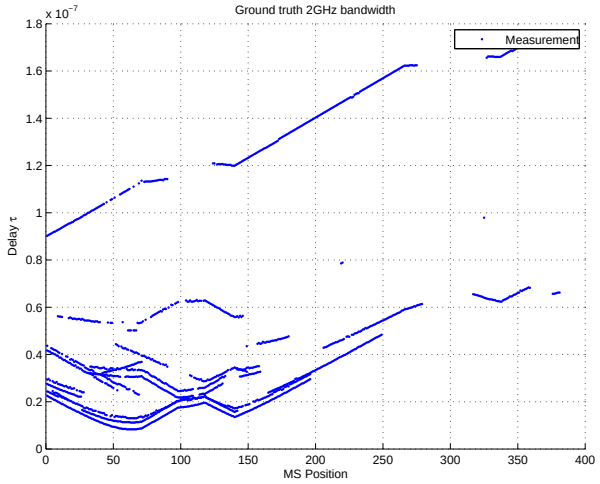

(b) Delay τ

Figure 5.24: Ground truth of real measurements

- In the amplitude domain, the clutter is within the limit of the maximum peak amplitude in the current CIR and the threshold defined by the peak extraction method. In the delay domain, the peak extraction method does not have such a constraint. Because of the physical effects in wave propagation, the amplitude attenuation grows with increasing delay τ and limits the range of where the clutter is located in the delay domain. For the UWB-channels, it can be assumed that clutter is often in the vicinity of the MPCs [KP03]. This can be observed in the input measurement set in Fig. 5.23(b) where the delay range of the measurements is limited, except for the MS positions where no LOS or rather no strong signal amplitude is dominant (MS Position $k = 280$ to $k = 320$).

- The assumption of a constant Poisson distributed number of clutter present over all time-steps is violated in the sense that there are strong fluctuations in the target cardinality in the ground truth compared to the input measurement set. The peak extraction method used extracts peaks from the CIR, if the amplitude is above a threshold relative to the maximum amplitude of the CIR and a maximum number of peaks. If there is no significant

LOS or other MPC component, amplitude peaks with low amplitude are added to the measurement set. These peaks are caused by diffuse scatterer or noise and will cause a heavy imbalance in the measurement to clutter ratio.

These violations lead to two significant effects in the result of the SMC PHD-Filter:

- If the SNR is low, the separability of target measurement and clutter measurement is not given. Then the update step of the PHD-Filter is incorrect, because at first particles are propagated to locations where there is clutter in the measurements. Then, in the update step, the target-measurement likelihood will be high. Thus, the posterior pdf is incorrect which results in wrong target state estimates. In [CRV08] this behaviour is treated by the assumption that measurements caused by a target state will have a high amplitude compared to measurements caused by clutter. The clutter distribution and the target-measurement likelihood are adapted to incorporate this. Furthermore, if the clutter distribution in the measurements does not match with the assumed clutter distribution of the PHD-Filter, clutter in the measurements might not be well suppressed by the PHD-Filter. In the implementations of the PHD-Filter, the clutter distribution is assumed to be uniform over the whole state-space. Therefore, the intensity κ_k of the clutter RFS is constant by design. In the measurement set used, clutter in the amplitude domain is located in the proximity of the amplitude peak extraction threshold (compare Fig. 5.23 with Fig. 5.24). The influence of received measurements with low amplitude should therefore be low in the update step of the PHD-Filter. This is only the case if the clutter probability is adjusted appropriately. An adapted target-measurement likelihood and an appropriate clutter probability distribution are not used here and are an open issue for further work.

- If the clutter parameter λ does not match well with the clutter present in the measurements, the filter performance of the PHD-Filter is low. Either too less targets are estimated or too much clutter is present in the outcome of the filter. This behaviour can be well observed in the result plotted in Fig. 5.25 for MS positions where the cardinality of the ground truth is zero (MS position $k = 280$ to $k = 320$) and the outcome of the SMC PHD-Filter is not. The cardinality is plotted in Fig. 5.26(a).

The cardinality of the estimated targets is significantly lower compared to the ground truth. This is caused by the conservative parameter setting of the SMC PHD-Filter. Focus has to be put on suppressing clutter in the filter output while maintaining "well"-shaped target tracks. The OSPA multi-target miss-distance is plot in Fig. 5.26(b). The high cardinality error of the filter outcome is penalized with a high miss-distance close to the cut-off value $c = 0.1$.

The labelled filter output is plotted in Fig. 5.27. The estimated targets originated form the LOS component are correctly associated to a single track. Also a MPC is tracked for the first few MS positions. Many isolated targets could not be associated with a target track, because the labelling-threshold of neighbouring targets is lower than the threshold B_{thresh}.

Parameter	**Value**
P_S	0.9
P_D	0.98
κ	$1/1000$
N_0	500
M	500
Measurement-target likelihood variance:	
$\sigma^2_{\alpha,\mathrm{L}}$	$7 \cdot 10^{-3}$
$\sigma^2_{\tau,\mathrm{L}}$	$5 \cdot 10^{-4}$
Particle birth variance:	
$\sigma^2_{\alpha,\mathrm{b}}$	1
$\sigma^2_{\tau,\mathrm{b}}$	1
$\sigma^2_{\Delta\alpha,\mathrm{b}}$	$2 \cdot 10^{-3}$
$\sigma^2_{\Delta\tau,\mathrm{b}}$	$2 \cdot 10^{-3}$
Process noise variance:	
$\sigma^2_{\alpha,\mathbf{n}}$	0
$\sigma^2_{\tau,\mathbf{n}}$	0
$\sigma^2_{\Delta\alpha,\mathbf{n}}$	$2 \cdot 10^{-3}$
$\sigma^2_{\Delta\tau,\mathbf{n}}$	$2 \cdot 10^{-3}$
Association threshold:	
B_{thresh}	$6 \cdot 10^{-1}$

Table 5.5: Parameter setting of SMC PHD-Filter - Measurement set: real

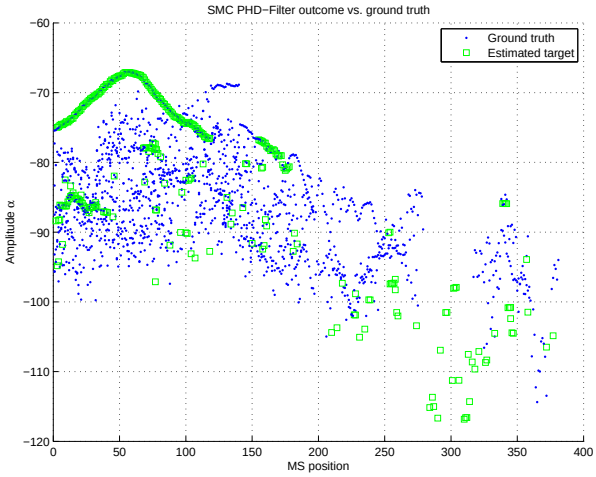

(a) Amplitude α

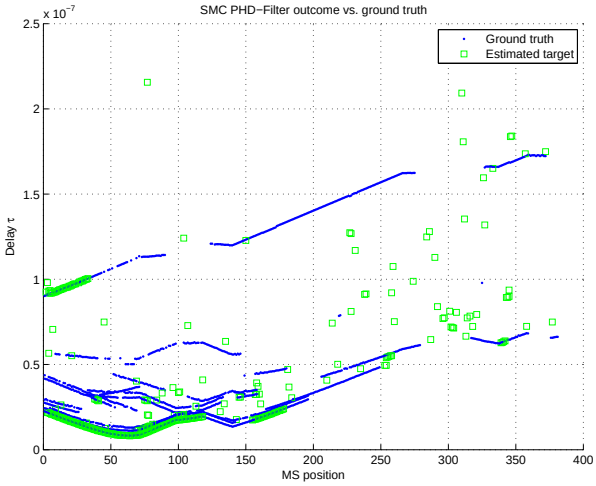

(b) Delay τ

Figure 5.25: SMC PHD-Filter: Ground truth vs. outcome of k-means clustering; Measurement set: real

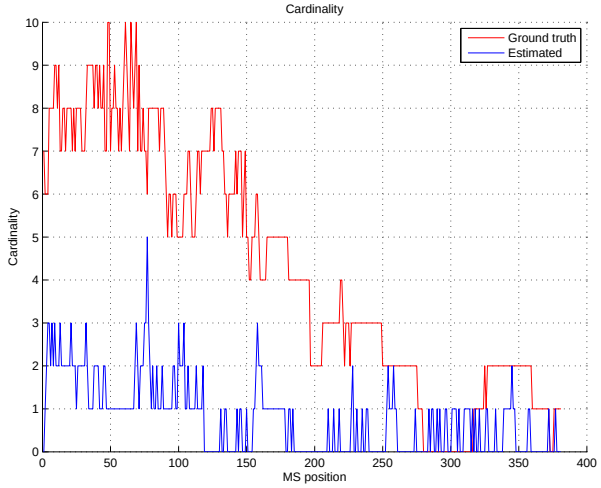

(a) Cardinality

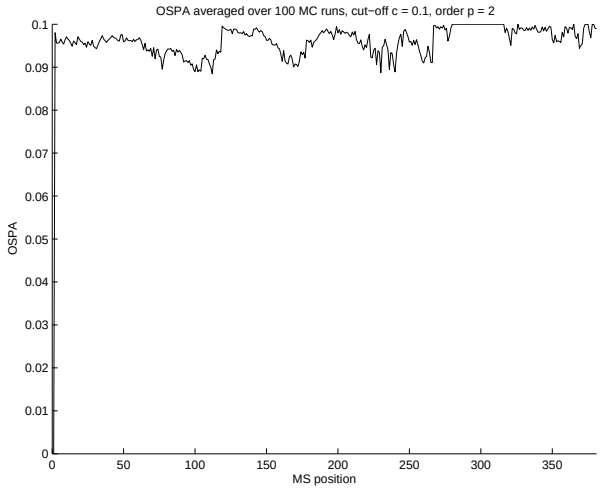

(b) OSPA distance

Figure 5.26: SMC PHD-Filter: OSPA miss-distance and cardinality; Measurement set: real

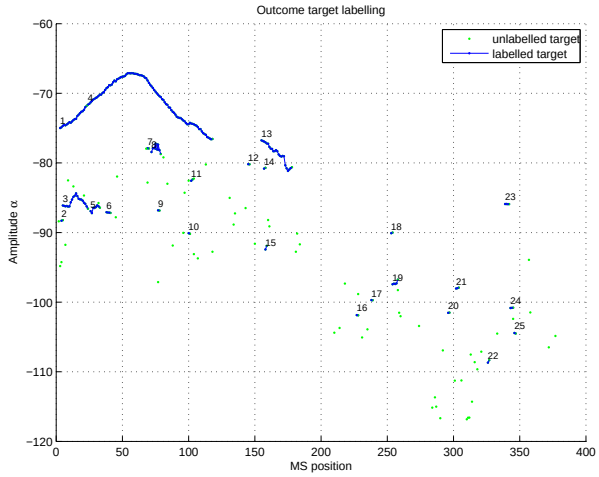

(a) Amplitude α

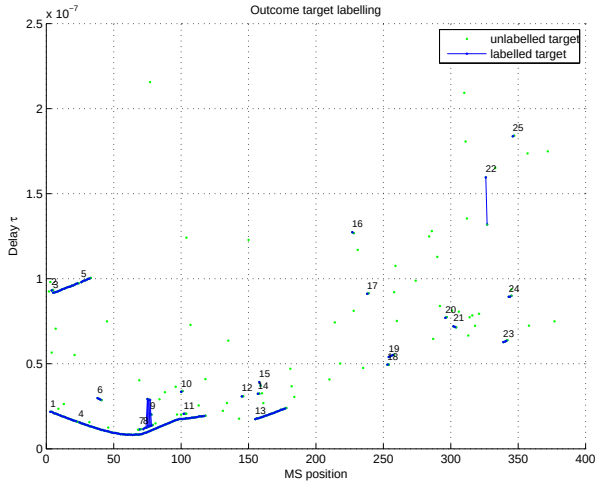

(b) Delay τ

Figure 5.27: SMC PHD-Filter: Labelled outcome; Measurement set: real

5.3.3 Performance Results for the GM PHD-Filter

The parameter setting of the GM PHD-Filter is given in Tab. 5.6. The filter design is again chosen very conservative, allowing only a small noise variance of the target states. The filter output is plotted in Fig. 5.28. The GM PHD-Filter is also able to track the LOS component, which has the highest SNR compared to the MPCs. For the first few MS positions no target state is estimated at the position of the LOS component. The weight of the corresponding GM components is simply to small to produce a filter output. After this initialization phase, the weight of the GM component following the LOS component is higher than 0.5 and a target state is output (see Alg. 7). Although the filter is restricted to constant velocity target dynamics it is able to track the non-linear state changes of the LOS component. In Fig. 5.28, also target states present for only one MS position can be observed. This can have several reasons:

- There are measurements caused by a target state which follows the linear state-space model, but only for a few MS positions. Then the GM PHD-Filter correctly produces an target estimate at its output. But due to the time it takes for the GM component to reach the weight threshold, the MPC is reported only for very few succeeding MS positions.
- The assumption of uniformly distributed clutter is violated. Measurements caused by clutter are concentrated in a small area of the state-space. This has the effect that the target-measurement likelihood in this area of the state-space used in the update step of the GM PHD-Filter is always high. Also the intensity of the clutter RFS is lower than the real one. Then the weight of a GM component increases although no target is present. Finally, the weight of a GM component exceeds 0.5 and a target state is output.
- The average number of measurements caused by clutter in the input measurement set does not follow a Poisson distribution. Therefore, the choice of a constant number of average clutter returns λ over all MS positions is incorrect. Either clutter will show up in the output of the GM PHD-Filter or too many target states will be suppressed by the filter and no or too less target states are output. The first is caused if κ is chosen too low and the latter if κ is too high. The restriction of $\lambda = \text{const.}$ is directly observable in Fig. 5.28 and in the cardinality plotted in Fig. 5.29(a). At MS position $k = 280$ to $k = 320$ the ground truth cardinality drops to zero whereas the cardinality of the GM PHD-Filter outcome does not. Incorrect target states are estimated and output from the GM PHD-Filter.

The OSPA multi-target miss-distance is plotted in Fig. 5.29(b). The miss-distance is always close to the cut-off value $c = 0.1$, due to the incorrect target estimate and the cardinality mismatch. Thus, the GM implementation of the PHD-Filter on the real measurement data set is weak. The cardinality of the estimated targets is higher compared to the SMC implementation. The cardinality of the ground truth is not higher than ten, but the GM PHD-Filter consequently over-estimates this. The estimated targets match with the ground truth despite some outliers, which have not been filtered by the filter.

A zoomed view of the labelled output is plot in Fig. 5.30. The choice of the association threshold B_{thresh} allows to suppress target outliers caused by clutter. Despite the LOS com-

ponent have estimated target tracks only have a small life-time. Too less target states, which follow the constant velocity model, are estimated in succeeding time-steps in the target tracks.

Parameter	**Value**
P_S	0.99
P_D	1
κ	15
Process noise covariance:	
$\sigma^2_{\tau,\mathrm{Q}}$	$1 \cdot 10^{-4}$
$\sigma^2_{\alpha,\mathrm{Q}}$	$5 \cdot 10^{-4}$
$\sigma^2_{\Delta\tau,\mathrm{Q}}$	$5 \cdot 10^{-4}$
$\sigma^2_{\Delta\alpha,\mathrm{Q}}$	$1 \cdot 10^{-3}$
Measurement noise covariance:	
$\sigma^2_{\tau,\mathrm{R}}$	$1 \cdot 10^{-5}$
$\sigma^2_{\alpha,\mathrm{R}}$	$1 \cdot 10^{-5}$
Birth RFS intensity:	
$\sigma^2_{\tau,\mathrm{B}}$	$1 \cdot 10^{-3}$
$\sigma^2_{\alpha,\mathrm{B}}$	$1 \cdot 10^{-3}$
$\sigma^2_{\Delta\tau,\mathrm{B}}$	$5 \cdot 10^{-2}$
$\sigma^2_{\Delta\alpha,\mathrm{B}}$	$5 \cdot 10^{-2}$
No. of GM components	81
Single GM component weight	1/81
Association threshold:	
B_{thresh}	$1 \cdot 10^{-1}$

Table 5.6: Parameter setting of GM PHD-Filter - Measurement set: real

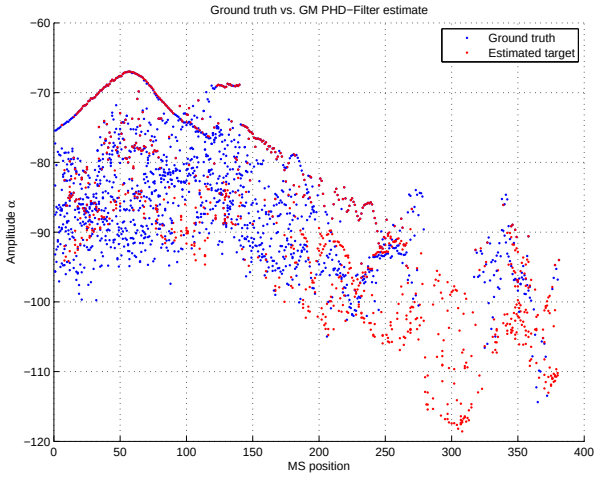

(a) Amplitude α

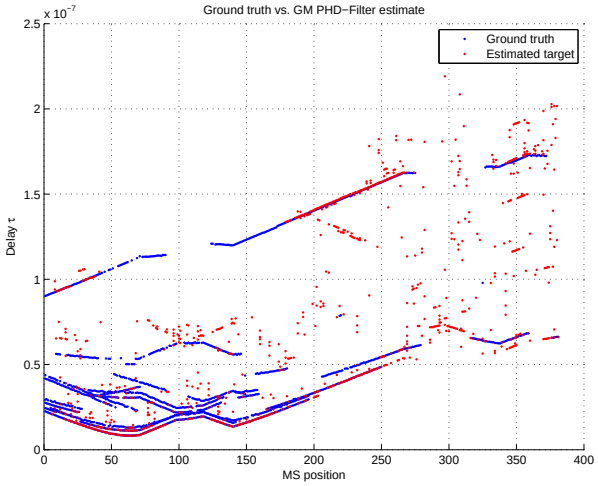

(b) Delay τ

Figure 5.28: Output GM PHD-Filter; Measurement set: real

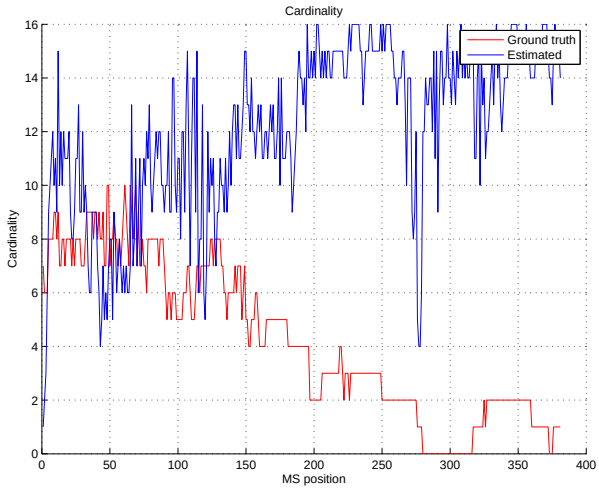

(a) Cardinality

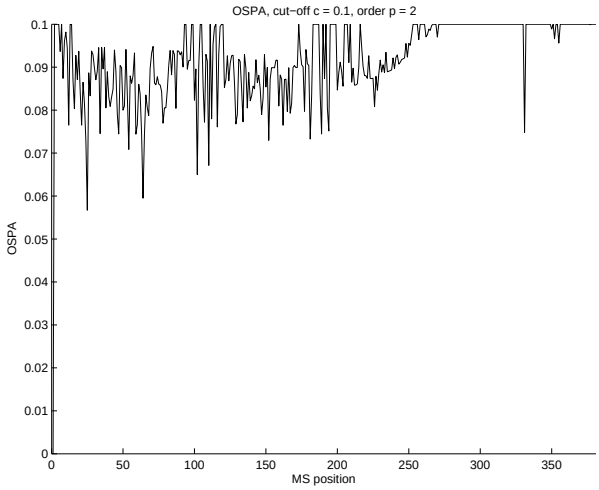

(b) OSPA distance

Figure 5.29: Outcome GM PHD-Filter; Measurement set: real

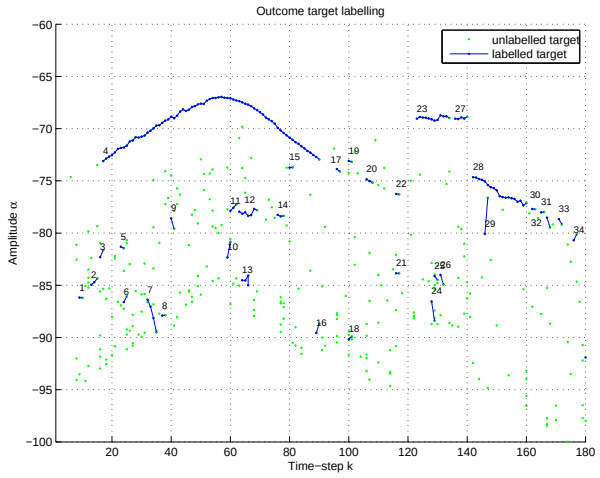

(a) Amplitude α

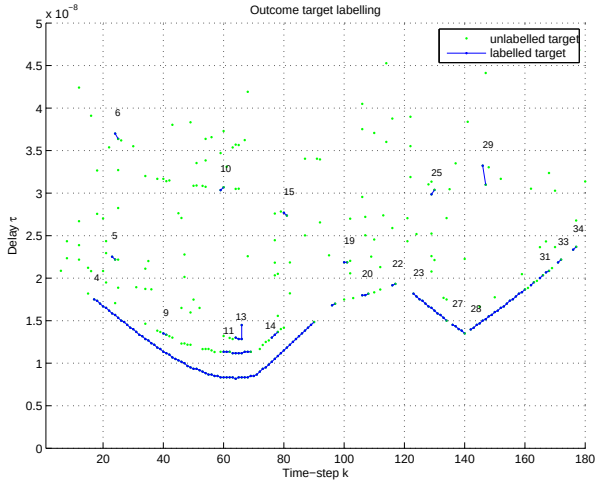

(b) Delay τ

Figure 5.30: GM PHD-Filter: Zoomed view of labelled outcome; Measurement set: real

5.3.4 Summary

Both the SMC PHD-Filter and the GM PHD-Filter are able to correctly estimate target states originated from the LOS component in areas where the SNR is high. This is due to the fact that the target movement fits quite-well with the constant velocity state-space propagation model used in the PHD-Filters. Small deviations can be reconcilabled by an increased process noise. If the SNR is low in both, the delay τ and the amplitude α domain, the PHD-Filter is not able to estimate valid target states, because then, the estimated PHD is not a valid approximation of the posterior pdf [Sid03]. For other MPCs present in the measurement set these conditions are to a great extend not fulfilled and too less target states are estimated or clutter remains at the output of the filter.

In the case of the SMC PHD-Filter, the estimated cardinality lags far behind the ground truth. The constant velocity model used in the PHD-Filter can not cope with the non-linear target dynamics present in the measurement set and leads to a low cardinality.

Despite the model mismatches, the GM PHD-Filter suffers to a greater extend from its restrictions. In the GM PHD-Filter the targets birth distribution is restricted to follow a GMM and the clutter distribution was assumed to be uniform. In the measurements, the MPC can appear anywhere in the state-space, but the clutter is accumulated in the α-domain at the proximity of the amplitude threshold of the peak extraction used in the preprocessing step. In the τ-domain it is located close to the MPCs. These distribution mismatches lead to a treatment of clutter in the way that it remains in the output of the filter. The cardinality is then also severely misestimated. The usage of the GM PHD-Filter only makes sense in areas where some prior knowledge of the target appearance is present. Also, the dynamic of the single targets have to follow the linear Gaussian assumptions made.

Because of this, the overall performance of both PHD-Filter implementations on the data set is not satisfying. Also, the linear constant-velocity state-space model used does not cope with the true target dynamics present in the data set. This results in a deterioration of performance. Furthermore, the true clutter distribution in the data set does not follow the assumptions of a uniform distribution made in the PHD-Filter.

6 Conclusion

Two types of PHD-Filter implementations have been evaluated both on simulated and on real measurement data. The PHD-Filter performs well if its constraints on the data set are not violated. For simulated measurement data, these constraints could easily be fulfilled. There, the PHD-Filter proofed to be a well-performing multi-source multi-target filter. The filter is in most cases able to estimate the target cardinality, even when there is a lot of clutter present in the measurements.

The PHD-Filter does not output the target states directly and avoids the data association problem. Target states have to be extracted from the PHD, the first moment of the multi-target posterior pdf.

The SMC PHD-Filter uses a sequential Monte-Carlo approach to approximate and propagate the PHD in time. The target states are then obtained with k-means clustering of the posterior particle representation. The filter is however not always able to suppress the whole clutter present in the measurement set. This results then in an incorrectly estimated cardinality and can lead to erroneous results of the clustering step of the SMC PHD-Filter, i.e. to incorrect target estimates. Estimated targets are assigned to target tracks with a simple labelling algorithm. This algorithm has problems concerning track continuity if single target states are not estimated. Despite this, the performance of the PHD-Filters is good even if the target movement shows mismatches with the constant-velocity model used. Then the particle number has to be increased to cope with this. This leads to a longer execution time of the filter iteration.

In the case of the GM PHD-Filter, the target movement is restricted to follow linear Gaussian dynamics. Furthermore, the target birth distribution has to follow a GMM. Then the filter pro-

vides a closed-form solution of the PHD recursion. The restrictions of the GM implementation of the PHD-Filter limit the field of application. If there is a mismatch in target dynamics, the GM PHD-Filter can still be used even though the performance degrades. If target appearance does not match with the given GMM birth distribution, targets will be hardly detected. Using equally spaced GM components over the whole state-space does not lead to a better performance. In cases where the restrictions of the GM implementation are fulfilled, the GM implementation is superior to the SMC implementation. Extraction of the targets state is easily done, because the GM components directly represent the targets mean and covariance. Furthermore, because target dynamic is restricted, also the output target tracks of the labelling procedure are very continuous.

In a real world scenario with non-linear target dynamic, a reasonable performance of the PHD-Filters is not given any more. The target dynamics present in the data set could not be tracked using the PHD-Filters with a constant velocity state-space model. However, if measurements are present in the measurement set originated from targets which follow these model assumptions, e.g. the LOS component, the filters are able to correctly estimate the target states.

In the case of the SMC PHD-filter, these model mismatches lead to an under estimation of the cardinality. The GM PHD-Filter suffers from its own restrictions: The mismatches of the clutter and birth distributions between measurement set and PHD-filter lead to a treatment of clutter in the way that it remains in the output of the filter. The cardinality is then also severely misestimated. The usage of the GM PHD-Filter only makes sense in areas where some prior knowledge of the target appearance is present. Also, the dynamic of the single targets have to follow the linear Gaussian assumptions made.

6.1 Further Work

The measurement set of the PHD-Filters consists only of the delay and amplitude value of the most strongest peaks to estimate the present MPCs. This might be a too big loss of information. Furthermore, the state-space model needs to be adapted to incorporate the non-linear dynamics of the MPCs. Then the GM PHD-Filter cannot be used any more. Non-linear implementations exist [VM06] and should be considered. We have seen in the measurements that the clutter is non-uniformly distributed over the state-space. The clutter model used needs to be adapted to fit with the model of the measurements. In the case of the GM PHD-Filter prior knowledge about the targets birth needs also to be incorporated. The PHD-Filter only propagates the first order multi-target moment in time. Propagating also the second order is in the single-target case comparable with the Kalman filter, but up to now computationally intractable. A step in this direction is the CPHD-Filter, which additionally to the PHD-Filter, propagates the cardinality distribution of the target state set [Mah07b]. Using this filter together with the adapted models of clutter, birth and the target dynamics might lead to the desired performance and makes the extraction of MPCs from the UWB-CIRs possible.

Bibliography

[AMGC02] M.S. Arulampalam, S. Maskell, N. Gordon, and T. Clapp. A tutorial on particle filters for online nonlinear/non-Gaussian Bayesian tracking. *Signal Processing, IEEE Transactions on*, 50(2):174 –188, 2002.

[BDW06] T. Bailey and H. Durrant-Whyte. Simultaneous localization and mapping (SLAM): part II. *Robotics Automation Magazine, IEEE*, 13(3):108 –117, 2006.

[BN07] Christopher M. Bishop and Nasser M. Nasrabadi. *Pattern Recognition and Machine Learning*, volume 16. SPIE, 2007.

[BSL95] Y. Bar-Shalom and X.-R. Li. *Multitarget-Multisensor Tracking: Principles and Techniques*. YBS, 1995.

[CB07] D.E. Clark and J. Bell. Multi-target state estimation and track continuity for the particle PHD filter. *Aerospace and Electronic Systems, IEEE Transactions on*, 43(4):1441 –1453, 2007.

[CPV06] D.E. Clark, K. Panta, and B.-N. Vo. The GM-PHD Filter Multiple Target Tracker. In *Information Fusion, 2006 9th International Conference on*, pages 1 –8, 2006.

[CRV08] D. Clark, B. Ristic, and Ba-Ngu Vo. PHD Filtering with target amplitude feature. In *Information Fusion, 2008 11th International Conference on*, pages 1 –7, 2008.

[DWB06] H. Durrant-Whyte and T. Bailey. Simultaneous localization and mapping: part I. *Robotics Automation Magazine, IEEE*, 13(2):99 –110, 2006.

[FMGW11] M. Froehle, P. Meissner, T. Gigl, and K. Witrisal. Scatterer and virtual source detection for indoor UWB channels. In *Ultra-Wideband (ICUWB), 2011 IEEE International Conference on*, pages 16 –20, 2011.

[HM02] J.R. Hoffman and R.P.S. Mahler. Multitarget miss distance and its applications. In *Information Fusion, 2002. Proceedings of the Fifth International Conference on*, volume 1, pages 149 – 155 vol.1, 2002.

[HRV11] K. Haneda, A. Richter, and P. Vainikainen. Experimental identification of an image source distribution on an indoor map. In *Antennas and Propagation (EUCAP), Proceedings of the 5th European Conference on*, pages 2646 –2650, 2011.

[Kal60] R E Kalman. A new approach to linear filtering and prediction problems. *Journal Of Basic Engineering*, 82(Series D):35–45, 1960.

[KP03] J. Kunisch and J. Pamp. An ultra-wideband space-variant multipath indoor radio channel model. In *Ultra Wideband Systems and Technologies, 2003 IEEE Conference on*, pages 290 – 294, 2003.

[Llo82] S. Lloyd. Least squares quantization in PCM. *Information Theory, IEEE Transactions on*, 28(2):129 – 137, 1982.

[MAGW11] P. Meissner, D. Arnitz, T. Gigl, and K. Witrisal. Analysis of an indoor UWB channel for multipath-aided localization. In *Ultra-Wideband (ICUWB), 2011 IEEE International Conference on*, pages 565 –569, 2011.

[Mah01] R.P.S. Mahler. Multitarget Moments and their Application to Multitarget Tracking. *Defense Technical Information Center OAI-PMH Repository (United States)*, page 34, 2001.

[Mah03] R.P.S. Mahler. Multitarget Bayes filtering via first-order multitarget moments. *Aerospace and Electronic Systems, IEEE Transactions on*, 39(4):1152 – 1178, 2003.

[Mah04] R.P.S. Mahler. "Statistics 101" for multisensor, multitarget data fusion. *Aerospace and Electronic Systems Magazine, IEEE*, 19(1):53 –64, 2004.

[Mah07a] R. Mahler. PHD filters of higher order in target number. In *Aerospace and Electronic Systems, IEEE Transactions on*, volume 43, pages 1523 –1543, october 2007.

[Mah07b] R.P.S. Mahler. *Statistical multisource-multitarget information fusion*. Artech House, 2007.

[Mol05] Andreas Molisch. *Wireless Communications*. John Wiley & Sons, 2005.

[Mol09] A.F. Molisch. Ultra-Wide-Band Propagation Channels. *Proceedings of the IEEE*, 97(2):353 –371, 2009.

[MSW10] P. Meissner, C. Steiner, and K. Witrisal. UWB positioning with virtual anchors and floor plan information. In *Positioning Navigation and Communication (WPNC), 2010 7th Workshop on*, pages 150 –156, 2010.

[PCV09] K. Panta, D.E. Clark, and Ba-Ngu Vo. Data Association and Track Management for the Gaussian Mixture Probability Hypothesis Density Filter. *Aerospace and Electronic Systems, IEEE Transactions on*, 45(3):1003 –1016, 2009.

[PVSD04] Kusha Panta, Ba-Ngu Vo, Sumeetpal Singh, and Arnaud Doucet. Probability hypothesis density filter versus multiple hypothesis tracking. *Signal Processing, Sensor Fusion, and Target Recognition XIII,*, 5429(1):284–295, 2004.

[RCV10] B. Ristic, D. Clark, and Ba-Ngu Vo. Improved SMC implementation of the PHD filter. In *Information Fusion (FUSION), 2010 13th Conference on*, pages 1 –8, 2010.

[Rei79] D. Reid. An algorithm for tracking multiple targets. *Automatic Control, IEEE Transactions on*, 24(6):843 – 854, 1979.

[Sid03] Hedvig Sidenbladh. Multi-target particle filtering for the probability hypothesis density. *CoRR*, cs.AI/0303018, 2003.

[Sim06] Dan Simon. *Optimal State Estimation: Kalman, H Infinity, and Nonlinear Approaches*. Wiley, Newark, NJ, 2006.

[SKA+08] T. Santos, J. Karedal, P. Almers, F. Tufvesson, and A.F. Molisch. Scatterer Detection by Successive Cancellation for UWB - Method and Experimental Verification. In *Vehicular Technology Conference, 2008. VTC Spring 2008. IEEE*, pages 445 –449, 2008.

[SKA+10] T. Santos, J. Karedal, P. Almers, F. Tufvesson, and A. Molisch. Modeling the ultra-wideband outdoor channel: Measurements and parameter extraction method. *Wireless Communications, IEEE Transactions on*, 9(1):282 –290, january 2010.

[SVL04] Simo Srkk, Aki Vehtari, and Jouko Lampinen. Rao-Blackwellized Monte Carlo Data Association for Multiple Target Tracking. *Information Fusion, Seventh International Conference on*, pages 583–590, 2004.

[SVL07] Simo Srkk, Aki Vehtari, and Jouko Lampinen. Rao-Blackwellized particle filter for multiple target tracking. *Information Fusion*, 8(1):2 – 15, 2007. Seventh International Conference on Information Fusion.

[SVV08] D. Schuhmacher, B.-T. Vo, and B.-N. Vo. A Consistent Metric for Performance Evaluation of Multi-Object Filters. *Signal Processing, IEEE Transactions on*, 56(8):3447 –3457, 2008.

[SW09] Yuan Shen and M.Z. Win. On the Use of Multipath Geometry for Wideband Cooperative Localization. In *Global Telecommunications Conference, 2009. GLOBECOM 2009. IEEE*, pages 1 –6, 2009.

[VM05] B.-N. Vo and W.-K. Ma. A closed-form solution for the probability hypothesis density filter. In *Information Fusion, 2005 8th International Conference on*, volume 2, page 8 pp., 2005.

[VM06] B.-N. Vo and W.-K. Ma. The Gaussian Mixture Probability Hypothesis Density Filter. *Signal Processing, IEEE Transactions on*, 54(11):4091 –4104, 2006.

[VS03] B.-N. Vo and S. Singh. Sequential Monte Carlo Implementation of the PHD Filter for Multi-target Tracking. pages 792–799, 2003.

[VVC06] B.-T. Vo, B.-N. Vo, and A. Cantoni. The Cardinalized Probability Hypothesis Density Filter for Linear Gaussian Multi-Target Models. In *Information Sciences and Systems, 2006 40th Annual Conference on*, pages 681 –686, 2006.

[WB01] Greg Welch and Gary Bishop. An Introduction to the Kalman Filter. *Design*, 7(1):1–16, 2001.

[YSK+08] Xuefeng Yin, G. Steinbock, G.E. Kirkelund, T. Pedersen, P. Blattnig, A. Jaquier, and B.H. Fleury. Tracking of Time-Variant Radio Propagation Paths Using Particle Filtering. In *Communications, 2008. ICC '08. IEEE International Conference on*, pages 920 –924, 2008.